https://doi.org/10.5194/egusphere-2026-1467
Preprint. Discussion started: 9 April 2026

Drivers of aerosol variability in the high Arctic: insights from integrated observations at Gruvebadet and Zeppelin (Ny-Ålesund)

Elena Barbaro[1], Francisco Ardini[2], Silvia Becagli[3], Stefano Bertinetti[4], Federica Bruschi[6], Giulia Calzolai[5], Alice Cavaliere[1], David Cappelletti[6,1], Stefano Crocchianti[6], Matteo Feltracco[7,8,1], Andrea Gambaro[7,1], Fabio Giardi[5], Stefania Gilardoni[1], Marco Grotti[2], Dominic Heslin-Rees[8], Radovan Krejci[9], Mery Malandrino[4], Matilde Mataloni[2], Simonetta Montaguti[10], Silvia Nava[11,5], Marco Paglione[10], Matteo Rinaldi[10], Chiara Ripa[1], Mirko Severi[3], Andrea Spolaor[1], Rita Traversi[3], Hilde Uggerud[12], Giulio Verazzo[1], Tessa Viglezio[1], Karl Espen Yttri[12], Wenche Aas[12], Mauro Mazzola[1]

[1]Institute of Polar Sciences, National Research Council of Italy (ISP-CNR), Venice, 30172, Italy;
[2]Department of Chemistry and Industrial Chemistry, University of Genoa, 16146 Genoa, Italy;
[3]University of Florence - Department of Chemistry "Ugo Schiff" Sesto Fiorentino (FI);
[4]Department of Analytical Chemistry, University of Torino, 10125 Torino, Italy;
[5]National Institute for Nuclear Physics, INFN-Florence, Sesto Fiorentino, 50019, Italy;
[6]Department of Chemistry, Biology and Biotechnology, University of Perugia, 06123 Perugia, Italy;
[7]Department of Environmental Sciences, Informatics and Statistics, Ca' Foscari University of Venice, 30172, Venice, Italy
[8]Italian National Agency for New Technologies, Energy and Sustainable Economic Development (ENEA), Casaccia Research Center, 00123, Rome, Italy
[9]Department of Environmental Science, Stockholm University, Stockholm, Sweden
[10]Institute of Atmospheric Sciences and Climate, National Research Council of Italy (ISAC-CNR), Bologna, 40129 Italy
[11]Department of Physics and Astronomy, University of Florence, Sesto Fiorentino, 50019, Italy
[12]NILU, Kjeller, 2007, Norway.

Correspondence to: Matteo Feltracco (matteo.feltracco@unive.it)

Abstract. This paper summarizes the main results from the scientific project "Boundary layer Evolution Through Harmonization of Aerosol measurements at Ny-Ålesund research stations" (BETHA-NyÅ), in which aerosol measurements of two Arctic atmospheric observatories located near Ny-Ålesund (Svalbard) at different elevations were harmonized: at the Gruvebadet atmospheric laboratory (61 m a.s.l.) and Zeppelin observatory (472 m a.s.l.). This approach allows for a better understanding of how atmospheric layering may affect the variability of aerosol observations in the Ny-Ålesund area. From February 2022 to March 2023, a coordinated sampling campaign enabled a direct comparison of optical, chemical, and physical aerosol properties, integrated with meteorological data from the Amundsen-Nobile Climate Change Tower. Results reveal a strong seasonal coherence between the two sites for two topical markers such as sulfate and ammonium, with clear evidence of the winter–spring Arctic Haze phenomenon. Local differences emerged mainly for biogenic tracers (e.g., arabitol and mannitol) which were detected at higher concentrations at Gruvebadet compared to Zeppelin observatory, highlighting the role of near-surface sources and aerosol stratification. The analysis of trace elements, lead isotopic ratios, and organic markers helped us to distinguish natural from anthropogenic contributions, confirming the dominant role of long-range transport and the persistence of isotopic signatures consistent with Eurasian sources. The systematic comparison across the two observatories

https://doi.org/10.5194/egusphere-2026-1467
Preprint. Discussion started: 9 April 2026

demonstrates the robustness of the harmonized protocol and emphasizes the importance of an integrated monitoring network for evaluating the evolution of atmospheric processes in the Arctic.

1 Introduction

The Arctic is undergoing the most severe effects of the current climate change, amplifying and driving changes elsewhere in the Earth system. In particular, the Arctic near-surface temperature is increasing about 2-3 times faster than the global average and it is called "Arctic Amplification" (Serreze and Barry, 2011). The peculiar feedbacks between climate forcings and environmental responses especially involve large changes in surface albedo, over land, sea and long-range transport patterns of air pollutants (IPCC, 2013). A detailed understanding of atmospheric processes at different scales can help to define the main causes of "Arctic Amplification". In this scenario, knowledge of the vertical structure of the Arctic Boundary Layer (ABL), which is the turbulent lowest part of the Arctic atmosphere, is essential because ABL can impact on the transport of different type of aerosols and consequent deposition on the glaciers and sea ice surfaces (Jozef et al., 2024).

The Svalbard archipelago is Norway's northernmost region and one of the northernmost land areas in the world. The Ny-Ålesund research settlement is located on the Brøgger Peninsula on the shore of Kongsfjorden, in western Spitsbergen, the largest island at Svalbard, and hosts several national and international research institutions with long-term monitoring programs and research projects. This site offers an excellent opportunity to investigate the ABL due to the co-location of three key facilities: the Gruvebadet Atmospheric Laboratory (GAL), the Zeppelin Observatory (ZEP), and the Amundsen-Nobile Climate Change Tower (CCT). GAL is located 800 m south-west of Ny-Ålesund, dedicated to the chemical and physical characterization of atmospheric aerosols, with continuous monitoring activities beginning in 2010, and are still ongoing (Barbaro et al., 2024; Becagli et al., 2019; Conca et al., 2019; Feltracco et al., 2020, 2021; Giardi et al., 2016; Grotti et al., 2024; Udisti et al., 2016). In addition, GAL has been the location for release of tethered balloons equipped with an optical particle counter (OPC), a black carbon (BC) monitor, and meteorological sensors to investigate size-resolved particle properties within and above the boundary layer (Mazzola et al., 2016).

ZEP is located at the top of Zeppelin Mountain (474 m asl), approximately 3 km from the coast of the fjord and 1 km from GAL. The monitoring activity is linked to several different international programmes and research infrastructures, such as EMEP (the European Monitoring and Evaluation Programme under LRTAP, UNECE), AMAP (Arctic Monitoring and Assessment Programme), ACTRIS (European Research Infrastructure for the observation of Aerosol, Clouds, and Trace gases), SIOS (Svalbard Integrated Arctic Earth Observing System), ICOS (Integrated Carbon Observation System) and WMO/GAW (World Meteorological Organization/Global Atmosphere Watch). Continuous monitoring has been carried out since 1989, although the first aerosol measurements in Ny-Ålesund date back to 1974 (Platt et al. 2022). The daily operation at the station is performed by the Norwegian Polar Institute (NPI), while NILU and Stockholm university (SU) are responsible for the scientific activities, depending on the type of measurement (Table 1). ZEP is less likely to be affected by local

https://doi.org/10.5194/egusphere-2026-1467
Preprint. Discussion started: 9 April 2026

anthropogenic sources than GAL due to its location and by local air flow phenomena such as katabatic winds (Ström, et al., 2009).

The CCT was installed in 2009, about 2 km west of Ny-Ålesund on the southern coast of Kongsfjorden. The 34 m high tower hosts standard meteorological sensors at different heights, sonic anemometers coupled with fast gas sensors, radiation sensors, as well as snow and ground sensors at its base. The CCT was conceived to host scientific experiments and instruments devoted to studying ABL dynamics under different atmospheric conditions (Mazzola et al., 2016).

Aerosol plays a relevant role on climate by scattering and absorbing the solar radiation and by influencing cloud formation (i.e. cloud condensation nuclei). Aerosol particles are transported from the middle latitude influencing the composition of the Arctic atmosphere, with consequent effects on cloud formation, albedo or sea ice. Several aspects remain poorly known, representing the challenge of the recent aerosol research. For example, organic compounds have notable consequences for atmospheric chemistry and cloud formation, but limited information about the sources of key compound classes such as sugars were produced. On the other hand, the positive forcing of black carbon (BC) is well known because it enhances light absorption processes in the atmosphere, especially in the Arctic, and after its deposition over the glaciers, where it triggers and accelerates melting processes. However, the dynamics of BC entertainment in the ABL are still a poorly understood process and may have a wide variability depending on local conditions (Gilardoni et al., 2020). Studying the ABL is crucial as even small changes in its thermodynamic structure or stability can strongly influence aerosol dispersion, cloud formation, and surface radiative balance. It plays a key role in regulating the exchange of energy, moisture, and aerosols between the surface and the free troposphere. These processes ultimately determine how aerosols affect Arctic amplification and ice–albedo feedback mechanisms (Gilardoni et al., 2020).

The key objective of BETHA-NyÅ project was to set up an aerosol measurement inter-comparison experiment between the GAL and ZEP observatories to assess how vertical gradient effects aerosol composition in the Arctic. Composition data from the two observatories were integrated with meteorological information from the CCT and radio soundings. Long-term harmonization of sampling strategies is highly beneficial for assessing how atmospheric layering affects the chemical signatures observed at different heights in the Arctic.

2 Material and methods

Ny-Ålesund is a unique location to investigate ABL processes thanks to the availability of two facilities at the same place but at different altitudes: GAL (78.918°N, 11.895°E) at 61 m above sea level and ZEP Observatory station (78.908°N, 11.881°E) at 472 m above sea level (Fig. 1) less than 2 km from each other. Moreover, data from the CCT enabled us to assess how local near surface processes influence boundary layer dynamics, thermal stratification, and surface-atmosphere interactions affect aerosol concentration, composition, and transport between the two monitoring sites.

The instrumental set-up and sampling parameters at GAL were adjusted to match, as closely as possible, the procedures used at ZEP. The harmonized protocol was implemented on 21 February 2022, and this paper presents results from the first sampling

https://doi.org/10.5194/egusphere-2026-1467
Preprint. Discussion started: 9 April 2026

period, which continued until March 2023; the protocol remains in use at present. Table 1 summarizes the harmonized measurement set-up at both sites.

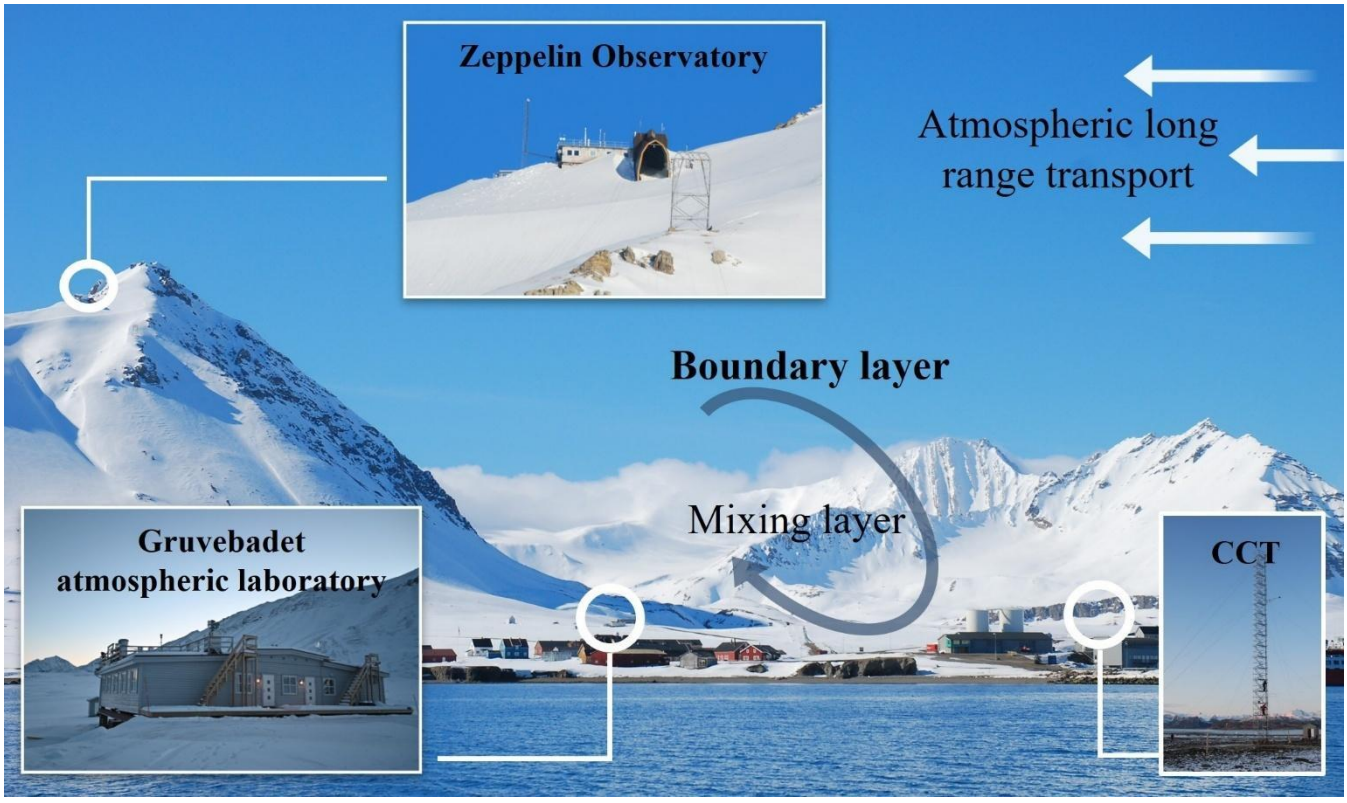

Figure 1. Sampling locations at Ny-Ålesund: Gruvebadet atmospheric laboratory (GAL), Zeppelin Observatory (ZEP) and Amundsen-Nobile Climate Change Tower (CCT).

Table 1. Summary of details of harmonized measurements in both sites: Gruvebadet atmospheric laboratory (GAL) and Zeppelin (ZEP) Observatory.

Measurements	GAL	ZEP
Absorption coefficient	Managing: ISP-CNR Sampler: aethalometer at seven wavelengths (AE33, Aerosol Magee Scientific), cut-off TSP Sampling resolution: 1 hour	Managing: SU Sampler: Multi Angle Absorption Photometer (MAAP, Magee Scientific Corporation), cut-off TSP Sampling resolution: 1 hour
Major inorganic ions	Managing: University of Florence	Managing: NILU Sampler: Three stage open filter face

https://doi.org/10.5194/egusphere-2026-1467
Preprint. Discussion started: 9 April 2026

	Sampler: PM_{10} low-volume sampler (TECORA Skypost), flow 38.3 L min^{-1} Filters: 47 mm diameter PTFE filters Sampling resolution: 24-48 hours	Filters: 47 mm diameter Teflon filters (Zefluor PFTE) Sampling resolution: 24 hours, change at 07:00 UTC.
Trace elements, isotopic and elemental analysis	Managing: University of Turin Sampler: PM_{10} high volume (TECORA Skypost), flow 150 L min^{-1} Filters: 90 mm diameter PTFE filters Sampling resolution: 1 week Managing: INFN Sampler: PM_{10} low-volume sampler (TECORA Skypost), 38.3 L min^{-1} Filters: 25 mm diameter ring-supported, stretched PTFE Sampling resolution: 1-2 days	Managing: NILU Sampler: $PM_{2.6}$ high-volume (DIGITEL DH-77), flow 43.8 L min^{-1} Filters: 150 mm diameter Whatman 41 Sampling resolution: 48 hours
EC/OC	Managing: INFN Sampler: PM10 low-volume sampler (TECORA Echo-PM), flow 38.3 L min^{-1} Filters: 25 mm diameter quartz fiber filters Sampling resolution: 1-2 days Managing: ISP-CNR Sampler: PM10 high-volume Andersen sampler (TE-6070 series, Tisch Environmental Inc.), flow 1140 L min^{-1} Filters: quartz fiber filters Sampling resolution: 1 week	Managing: NILU Sampler: PM_{10} Digitel high-volume sampler (DH-77, DIGITEL), flow 666 L min^{-1} Filters: Quartz fiber filters (WHATMAN 40 QM-A) Sampling resolution: 1 week
Organic tracers	Managing: ISP-CNR Sampler: PM10 high volume Andersen sampler (TE-6070 series, Tisch Environmental Inc.), flow 1140 L min^{-1} Filters: quartz fiber filters Sampling resolution: 1 week	Managing: NILU Sampler: PM_{10} Digitel high-volume sampler (DH-77, DIGITEL) Filters: Quartz fiber filters (WHATMAN 40 QM-A) Sampling resolution: 1 week

https://doi.org/10.5194/egusphere-2026-1467
Preprint. Discussion started: 9 April 2026

2.1. Sampling at Gruvebadet atmospheric laboratory and sample processing

Gruvebadet atmospheric laboratory (GAL) is located 800 m from Ny-Ålesund at an elevation of 61 m above sea level. The aerosol observations are conducted by CNR-ISP together with several Italian universities (Ca' Foscari University, Universities of Florence, Genoa, and Turin) and research institutions, such as National Institute of Nuclear Physics (INFN).

An aethalometer at seven wavelengths (AE33, Aerosol Magee Scientific) was installed to measure the absorption coefficient (σ_{abs}) and it is managed by ISP-CNR. Absorption data were corrected for multiple scattering using a correction coefficient (C) (Yus-Díez et al., 2021). Absorption coefficients at 530 nm were derived from the coefficient measured at 520 nm and using the Ångström Absorption Exponent (AAE) derived from the seven measured wavelengths. The scattering coefficient (σ_{sca}) at 530 nm was measured using a single wavelength integrating nephelometers (M903, Radiance Research, USA). Both σ_{abs} and σ_{sca} were averaged at one-hour time resolution.

A low-volume sampler (TECORA Skypost), managed by Florence University, collected one-to-two-day PM_{10} aerosol samples on 47 mm diameter PTFE filters (Pall Corporation and Cobetter Filtration Group). These filters were used to define PM_{10} mass and ionic composition. These samples were prepared under a laminar flow hood in Florence and shipped to Ny-Ålesund; after sampling, the filters were stored in a freezer at "Dirigibile Italia" Station and then shipped back to Florence together with field blanks. The filters were cut into two parts; one half is archived for further analysis while the other half is devoted to ion chromatographic analysis. The PM_{10} mass was determined by weighing the filter before and after the sampling using a five-digit microbalance (Sartorius ME235P). The filters were conditioned for 48 h (25 °C and 50% RH) before weighing. The portion of the filter devoted to chemical analysis was diluted with 10 mL of ultrapure water (18 MΩ·cm, Millipore MilliQ grade) and extracted in an ultrasonic bath for 20 minutes. Ion composition was measured by two Ion Chromatographic systems performing the analysis of inorganic anions and inorganic cations. The detailed procedure is described in Becagli et al. (2011). For all the parameters reproducibility on real samples was better than 5%, and filter blanks were found to be lower than the detection limit.

An Echo Hi-Vol sampler (TCR Tecora, 150 L min^{-1} with a week resolution) was used to collect PM_{10} samples on hydrophilic PTFE filters (H100A090C, 90-mm diameter, efficiency > 99% for 0.3 µm particles; Advantec MFS, Dublin, CA, USA). These samples were split into two different sections. The University of Genoa performed the determination of lead content and isotope ratios, while trace elements and rare earth elements were determined by the University of Turin.

A quarter of each PM_{10} high volume filter for trace elements analysis and Pb isotopic analysis underwent microwave-assisted digestion using a vessel-inside-vessel method, following EU air quality monitoring standards. Filters were cut with ceramic scissors pre-washed with acidic solution. The digestion was carried out at 220 °C with a mixture of HNO_3, H_2O_2, and high-purity water (HPW). Post-digestion, solutions were filtered, cleaned, and diluted to 10 mL. All steps occurred in a clean Class-100 laminar flow hood. Reagent blanks and sample blanks (from transported blank filters) were used to correct background contamination. Instrumental blanks and calibration checks ensured analytical accuracy, with <5% relative standard deviation per element. Certified Reference Material (NIST 1648a) confirmed recoveries of over 80% for most elements. All details about

https://doi.org/10.5194/egusphere-2026-1467
Preprint. Discussion started: 9 April 2026

the sample processing are reported by Conca et al. (2019). The elemental quantification was performed by an iCAP PRO XP ICP-OES (Thermo Fisher Scientific, Waltham, MA, USA), an Element 2 SF-ICP-MS (Thermo Fisher Scientific) and an 8900 ICP-MS/MS (Agilent, Santa Clara, CA, USA) according to the element concentrations.

The PM_{10} high volume samples for lead isotopes were analyzed as described in previous works (Bazzano et al., 2015; Grotti et al., 2023). Specifically, after performing the digestion, the samples were diluted to 10 mL with ultrapure water (Milli-Q from Merck Millipore) and analyzed by inductively coupled plasma mass spectrometry using a NexIon 2000 ICP-MS unit (Perkin Elmer, Waltham, MA, USA) for the determination of lead content and isotope ratios.

The concentration of Al was measured by inductively coupled plasma atomic emission spectrometry (Vista PRO Varian, Springvale, Australia) and used to calculate the enrichment factors (EFs) following the equation:

$$EF = (Pb/Al)_s/(Pb/Al)_{UCC} \quad (1)$$

Here, $(Pb/Al)_s$ is the ratio measured in each sample and $(Pb/Al)_{UCC}$ is the mean ratio for the upper continental crust (2.195 10-4) (Hans Wedepohl, 1995).

Another low-volume sampler (TECORA Skypost), managed by INFN, collected one day PM_{10} aerosol samples to define the elemental composition. The sampler was customized with a reducing sampling spot inlet, designed and realized at INFN Florence in order to get a sample deposit of about 2.1 cm diameter. The use of this reducer enhances the sensitivity of the analytical technique, namely Particle Induced X-ray Emission (PIXE), as it is sensitive to the areal density of the sample, thus it benefits from an increased concentration of the sample.

PM_{10} samples for elemental determination using PIXE were analyzed without any sample pre-treatment, thus minimizing any contamination risk. They were bombarded with a 3 MeV proton beam extracted in air using the set-up dedicated to environmental analyses at the INFN-LABEC 3MV Tandetron accelerator (Chiari et al., 2021). Spectra of the emitted x-rays were analysed using the GUPIXWIN code (Campbell et al., 2021), and to get the areal concentrations of the elements with Z>10. Atmospheric concentrations were then obtained multiplying the areal density for the deposit area and dividing for the sampled air volume.

A sampling strategy configuration with a flow-reducing sampling spot inlet was used for collecting samples for elemental (EC) and organic carbon (OC) analysis (Caiazzo et al., 2021). A low volume sampler (Tecora Echo-PM), equipped with reducers, was used to collect PM_{10} samples on 25 mm diameter quartz fiber filters. Before sampling, each 47 mm filter was punched to obtain a 25 mm diameter filter, which was then placed in the sampler and used for aerosol collection. The remaining outer portion of the 47 mm filter was kept and treated as a blank corresponding to each sample. After sampling, a 1.5 cm^2 punch was taken from the exposed 25 mm filter for analysis. An equivalent 1.5 cm^2 punch was also taken from the corresponding 47 mm blank corona. Both punches were analyzed by thermal-optical analysis (Sunset Laboratory Inc, USA), using the NIOSH-870 (Quartz of the National Institute for Occupational Safety and Health) protocol. It has been selected because this protocol provides better agreement between EC measured on washed and untreated quartz filters compared to other available thermal protocols (Giannoni et al., 2016, and references therein) and this is especially important for samples where the amount of EC

https://doi.org/10.5194/egusphere-2026-1467
Preprint. Discussion started: 9 April 2026

is very low. The value of every blank filter was subtracted from the corresponding sample, in order to get an accurate estimation and subtraction of the blank values (EC was always below the Detection Limit in blank filters).

EC/OC measurements at ZEP were performed using pre-fired (850 °C; 3 h) quartz fiber filters (Pallflex Tissuquartz 2500QAT-UP; 150 mm in diameter) weekly collected by Digitel PM10 high-volume sampler (Yttri et al., 2024). Thermal–optical analysis (TOA) was carried out using the Sunset Laboratory, Inc., OC/ EC aerosol analyzer, operating the instrument according to the EUSAAR-2 temperature program (Cavalli et al., 2010). To fully harmonise the monitoring procedures among ZEP and GAL, the same analytical protocol was used on the weekly samples at GAL, and ECOC analyser by Sunset Lab. Inc. was used as well. Samples collected according to the EC/OC monitoring ongoing since 2011 were measured according to the NIOSH-870 thermal protocol (i.e. according to the protocol in use since 2011), to compare and harmonise the data series.

A PM_{10} high volume Andersen sampler (TE-6070 series, Tisch Environmental Inc.) was used at a flow rate of 68 m^3 h^{-1} to collect aerosol samples on quartz fiber filters with a temporal resolution of 7 days. In these samples, ISP and Ca' Foscari University usually determine water soluble organic compounds. In particular, we reported here the results of sugars composition such as levoglucosan like biomass burning tracer or arabitol and mannitol, like fungal spores' markers. In addition, EC and OC determination was also performed by INFN using these samples to obtain an intercomparison between two instruments at GAL and also with ZEP samples. As EC and OC are quantified in ZEP samples using the EUSAAR2 thermal protocol, this was also applied to these GAL samples. Blank values were evaluated as the average on different blank filters (also in this case, EC was always below the Detection Limit in blank filters).

Monosaccharides (arabinose, fructose, galactose, glucose, mannose, ribose, xylose), sugar alcohols (erythritol, mannitol, arabitol, sorbitol, xylitol, maltitol, galactitol) and mono saccharide anhydrides (levoglucosan, mannosan and galactosan) were analyzed in weekly filter samples collected with Andersen high volume PM_{10} sampler. A quarter of each filter was extracted with 15 mL ultrapure water following the already validated procedure (Feltracco et al., 2020). The analytical determination was performed using two published methods through ion chromatograph (Thermo Scientific™ Dionex™ ICS-5000, Waltham, US) coupled to a single quadrupole mass spectrometer (MSQ Plus™, Thermo Scientific™, Bremen, Germany) (Barbaro et al., 2015).

Anhydrosugars and sugar alcohols were also determined in the samples collected at ZEP using Digitel high volume PM_{10} sampler. The analytical determination was carried out using ultra-performance liquid chromatography (UPLC) (Vanquish UHPLC, Thermo Fisher Scientific) in combination with Q Exactive™ Plus Orbitrap (Thermo Fisher Scientific). Filter punches (2×1.5 cm^2) were extracted with 2 mL tetrahydrofuran (THF) following by evaporation and purification (Yttri et al., 2024).

2.2 Zeppelin Observatory sampling and processing

The ZEP Observatory is owned and managed by the Norwegian Polar Institute. It is located on Mount Zeppelin on the 20 km long and 10 km wide Brøggerhalvøya, 2 km south of Ny-Ålesund.

The absorption coefficient (σabs) measurements reported were recorded using a Multi Angle Absorption Photometer (MAAP, Thermo Fisher Scientific) at ZEP. The instrument is operated by Stockholm University (SU) at standard flow 1 m^3 $hour^{-1}$ and

https://doi.org/10.5194/egusphere-2026-1467
Preprint. Discussion started: 9 April 2026

connected to a whole air inlet designed according to ACTRIS recommendations for sites often embedded in clouds (https://www.actris-ecac.eu/). The MAAP of ZEP provides absorption coefficients at 637 nm, which were converted to 660 nm following the methodology described by Müller et al. (2011). Absorption at 530 nm was then estimated assuming an AAE of 1. The eBC concentrations are calculated using instrument default MAC value 6.6 m^2 g^{-1}. Major ions are determined upon sampling with a three-stage filterpack using a devoted NILU filter holder system designed for sampling of particles and gaseous compounds (Aas et al., 2025). The first stage in the air stream is a Zeflour (2 µm) filter used to collect the airborne particles containing sulphate, ammonium, nitrate, sodium, calcium, potassium, chloride. The second stage is a filter (Whatman 40) impregnated with KOH so to collect HNO_3, SO_2, HNO_2, HCl, and other volatile acidic compounds. The third stage is an acid-impregnated (oxalic acid) filter (Whatman 40), used to absorb alkaline air components such as ammonia. For the nitrogen species, the sum of the concentration of the species in the gaseous and particulate phase is reported. Namely, for ammonium, concentration reported in the database equals the sum of ammonium collected on the aerosol front filter and ammonia collected on the acid-impregnated filter. Since the filterpack sampler is not equipped with an inertial impactor but a cylindrical vertical air intake, the sampling efficiency for large particles (such as mineral dust, sea spray droplets) is reduced and size cut-off is approximately PM_{10} except for strong sea salt episodes characterised by large particles. After exposure, the aerosol filters (first stage of the pack) undergo an ultrasonic treatment with water in order to obtain a complete extraction before analysis. The alkaline-impregnated filter is extracted by a hydrogen peroxide solution in order to oxidize any remaining sulphite to sulphate while the third stage (acid-impregnated filter) is extracted by a HNO_3 solution. All the ions are analysed using Ion Chromatograph.

Sampling of trace elements is done using a Digitel high-volume air sampler with a $PM_{2.6}$ cut-off, and samples are collected on a weekly basis, using Whatman grade 41 filter papers for 48 hours with an airflow rate of 43.8 m^{-3} $hour^{-1}$. The filters are digested with nitric acid by Ultraclave, a microwave-based decomposition technique. Identification and quantification are performed by ICP-MS, and In is used as an internal standard.

Details of the monitoring of at ZEP are found in the annual reports for the Norwegian Environmental agency; Aas et al. (2025) includes inorganic and organic components, while Halvorsen et al. (2025) describe the monitoring programme of trace elements.

2.3 Air mass back trajectories analysis and source regions classification

240 hours long back-trajectories reaching Ny-Ålesund on hourly basis were computed using the off-line, Linux based version 5.3.2 of the Hysplit code (Stein et al., 2015). For every hour, trajectories reaching the site at 50, 500, 1000 and 3000 m a.g.l. were calculated in the days ranging from 1st January 2022 to 31st December 2023. This is a standard procedure in our lab which allows us to build up a consistent database of BT in relevant receptor sites for successive uses of any type.

The meteorological data supplied to the program were Global Forecast System (GFS) at 0:25x0.25° resolution, downloaded in the "ARL packed" format from the US National Oceanic and Atmospheric Administration (NOAA) Air Resources Laboratory (ARL) database.

https://doi.org/10.5194/egusphere-2026-1467
Preprint. Discussion started: 9 April 2026

Trajectories frequencies, computed as the number of endpoints contained in each cell of a 1x1° lat/lon grid for each trajectory reaching the receptor at 50 m a.g.l., were plotted for time ranges matching the sampling periods.

NASA FIRMS MODIS satellite (combined Aqua and Terra) data (NASA-FIRMS, 2025) were downloaded and projected onto the frequencies plot as red circles whose diameter was proportional to the pixel fire radiative power. For each sample, fires occurring on a time range including the sampling period and the preceding 10 days were considered.

3. Results and discussion

This section presents a comprehensive analysis of the atmospheric conditions and their variability in the Kongsfjorden region of Svalbard, from February 2022 to March 2023 at the two observatories. An overview of the meteorological and radiative conditions is reported in the Supplementary Material (Sec. S1.1) while the results for atmospheric composition is reported in the following Subsections.

https://doi.org/10.5194/egusphere-2026-1467
Preprint. Discussion started: 9 April 2026

3.2 Aerosol optical properties

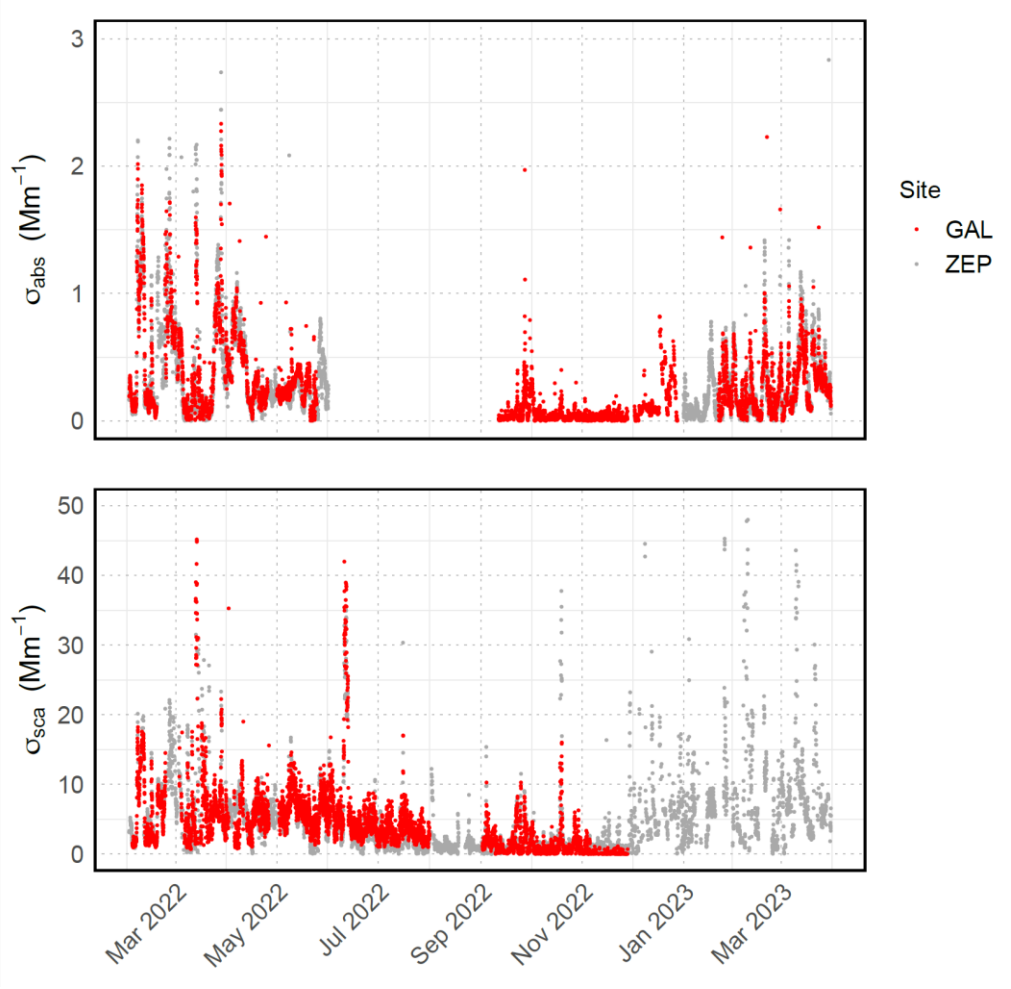

Figure 2. Aerosol absorption coefficients (top) and scattering coefficients (bottom) at 530 nm at GAL (in red) and at ZEP (in gray). A limited number of datapoints with absorption coefficient above 3 Mm^{-1} and with scattering coefficient above 50 Mm^{-1} are not shown in the figure.

Figure 2 shows the absorption and scattering coefficients at 530 nm measured at GAL and ZEP. In the cold season (November to April), the median scattering coefficients were 5.5 Mm^{-1} (IQR: 2.6 – 8.5 Mm^{-1}) at ZEP and 4.2 Mm^{-1} (IQR: 1.6-7.3 Mm^{-1}) at GAL, while in the warm season (May to October) they decreased to 1.6 Mm^{-1} (IQR: 0.8 – 3.6 Mm^{-1}) at ZEP and to 3.1 Mm^{-1} (IQR: 1.2 – 5.3 Mm^{-1}) at GAL. The medians of the absorption coefficient were 0.22 Mm^{-1} (IQR: 0.10 – 0.51 Mm^{-1}) at ZEP and 0.19 Mm^{-1} (IQR: 0.09 – 0.44 Mm^{-1}) at GAL, and 0.22 Mm^{-1} (IQR: 0.16 – 0.29 Mm^{-1}) at ZEP and 0.05 Mm^{-1} (IQR: 0.02 – 0.21 Mm^{-1}) at GAL, in the cold and warm season, respectively. The interquartile range reveals higher absorption coefficients

https://doi.org/10.5194/egusphere-2026-1467
Preprint. Discussion started: 9 April 2026

during the cold season at both sites, a seasonality that is attributed to air mass transport from mid-latitudes and the Arctic haze phenomenon (Gilardoni et al., 2023; Stohl, 2006a).

The comparison of two observatories based on parallel measurements of absorption coefficients and scattering coefficients conducted during the study period showed that the differences are centred around zero (Fig. S3).

The accuracy of the absorption coefficient measurements, as reported by the manufacturers, is 0.05 Mm^{-1} for AE33 data (1-hour averages) and 0.1 Mm^{-1} for MAAP measurements (30 min averages). Asmi et al. (2021) observed that in ambient conditions the two instruments can measure coefficients as low as 0.012 Mm^{-1}. Considering this value as the uncertainty level, the absolute value of the difference between the measurements would be significant if larger than 0.036. About 45% of the time, the difference of the absorption coefficients between the two sites was below this value.

For the integrating nephelometer, a systematic uncertainty below 10% is generally considered (Anderson et al. 1998). Assuming an uncertainty of 5% to be conservative, this would correspond to about 0.1 – 0.25 Mm^{-1}, depending on the period. During the cold and the warm season, the difference between the scattering coefficient was not significant (lower than 3 times the combined uncertainties) for 61% of 40% of the time, respectively.

The comparison of the optical properties reported (Fig. 2) indicates that the two sites observed similar air masses and/or experienced similar processes for about half of the time during the investigated period.

3.3 Comparison of seasonal trends of sulphate and ammonium between GAL and ZEP

The presented data set covers the entire year 2022 and approximately half of 2023 (1st January 2022 to 27th June 2023). This period includes the full BETHA-NyÅ project, as well as several months before and after, in order to provide an annual overview of the temporal trends.

Sulphate and ammonium, as key components of Arctic Haze, exhibit a pronounced seasonal pattern, with a broad maximum beginning in winter (most likely in December) and lasting until June or July, depending on the species (Fig. 3). Thereafter, a relatively flat pattern is observed during summer and autumn.

Sulphate, in particular, shows remarkably similar temporal behaviour and absolute concentrations at GAL and ZEP throughout the study period (Fig. 3a). The Arctic Haze period is clearly identifiable at both sites. In 2022/2023, sulphate concentrations peak in March-April and return to background levels (defined as the median over the entire study period) around mid-June at GAL and approximately one month later at ZEP. Interestingly, the onset of the winter increase differs between the two sites, beginning in early December at ZEP and in mid-January at GAL. Despite this offset, the highest peaks at both sites occur in March and April, often on the same days.

The difference in the timing of the onset and decline of the sulphate maximum may be related to the sites' relative position with respect to the boundary layer during early winter and early summer. While GAL is consistently located within the boundary layer (Rader et al., 2021), ZEP may at times represent conditions of the lowermost free troposphere, although it is most frequently influenced by the boundary layer air masses (Tunved et al., 2013). In terms of absolute concentrations, the agreements between the two sites are striking, despite differences in sampling methodologies. This suggests a high degree of

https://doi.org/10.5194/egusphere-2026-1467
Preprint. Discussion started: 9 April 2026

robustness in the measurements. Median concentrations are very similar (203 ng m^{-3} at GAL and 220 ng m^{-3} at ZEP), as are the averages over the entire study period (381 ng m^{-3} at GAL and 395 ng m^{-3} at ZEP). In contrast, variability appears to be greater at ZEP.

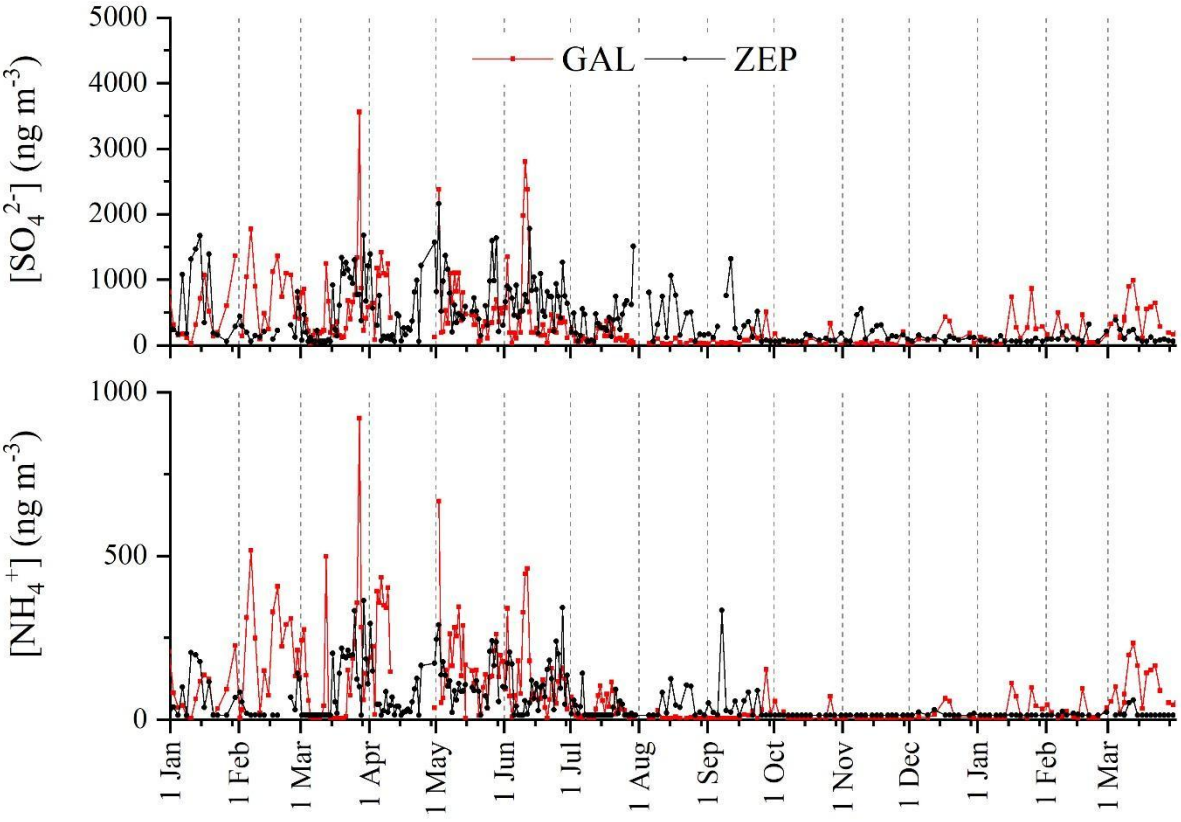

Figure 3. Comparison of seasonal trends of sulphate (a) and ammonium (b) at GAL and ZEP from Jan 2022 to Jun 2023.

Another parameter that can serve as an indicator of anthropogenic influence, including Arctic Haze, is ammonium. The temporal profiles of ammonium at the two sites are similar in terms of seasonal behavior (Fig. 3b), with the highest concentrations observed between January and May-June in both years at both sites. A closer inspection of the plots shows that, unlike sulphate, the broad concentration maximum ends at approximately the same time at both sites, while the onset is delayed by about one month at GAL compared to ZEP (mid-January vs. early December).

The similar behavior of sulphate and ammonium is consistent with the neutralization of sulphuric acid by ammonia. The extent of this process is illustrated in Fig. S4, which shows the linear correlation between sulphate and ammonium at GAL and at

https://doi.org/10.5194/egusphere-2026-1467
Preprint. Discussion started: 9 April 2026

ZEP. Both correlations are statistically significant at the 99% confidence level, considering the correlation coefficients (R^2=0.838 at GAL and R^2=0.407 at ZEP) and the large number of data points (> 300 at each site). While the data at ZEP appear quite scattered, GAL exhibits a strong linear relationship between the two species. Notably, the slope of the regression line is approximately 3.6 at both sites, indicating that they are influenced by similar dominant sources of sulphate and ammonium.This also suggests that, for these secondary species, GAL is representative of long-range transport processes despite being located at sea level.

The slope value lies between 2.66 and 5.39, corresponding to the sulphate-to-ammonium mass ratios expected for the formation of NH_4HSO_4 and $(NH_4)_2SO_4$, respectively. This indicates that, on average, sulphuric acid is largely neutralized by ammonia, forming a mixture of NH_4HSO_4 and $(NH_4)_2SO_4$. Previous studies in Ny-Ålesund (Giardi et al., 2016; Udisti et al., 2016, 2020) showed that sulphate is mainly present as ammonium salt, particularly during spring and summer. Those studies, focused on individual years (2013 and 2014), reported lower summer sulphate/ammonium ratios, approximately 2.66, consistent with complete neutralization to $(NH_4)_2SO_4$. However, long term data (2010–2019) reported by Traversi et al. (2021) show generally higher ratios at ZEP compared to GAL. Given that sulphate concentrations are similar at both sites while ammonium concentrations are lower at ZEP, the difference in the ratio is primarily driven by ammonium. GAL may be more influenced by local ammonia sources from surface emissions and seabird colonies, as suggested for the Canadian Arctic by Wentworth et al. (2016).

Considering the SO_4^{2-}/NH_4^+ ratio (w/w) at GAL and ZEP over the investigated period (Fig. S5), average values are higher at ZEP than at GAL (9.8 vs. 7.8), as are background values (6.6 vs. 4.1). This pattern is consistent with the long-term observations reported by Traversi et al. (2021). At ZEP, the highest ratios occur during winter-spring period, likely associated with Arctic Haze. In contrast, GAL shows a narrower maximum in March 2022 and April 2023, again, likely linked to Arctic Haze, but also a frequent occurrence of elevated ratios in summer and autumn.

This summer-autumn enhancement as GAL cannot be attributed to additional biogenic sulphur sources, as MSA exhibits a distinct seasonal pattern with a cleat maximum from May to August (Becagli et al., 2019; Park et al., 2021), which does not explain elevated values from July into winter. The observed difference may instead reflect local sulphuric acid sources affecting GAL during summer and/or analytical artifacts related to differences in detection limits between the two sites.

3.4 Elements composition

34 elements (Na, K, Mg, Ca, Al, Sc, Ti, V, Cr, Mn, Fe, Co, Ni, Cu, Zn, As, Sr, Y, Nb, Mo, Cd, Ba, La, Ce, Pr, Nd, Sm, Dy, Er, Tm, Yb, Hf, and Pb) were analysed in PM_{10} filter samples collected at GAL. Their concentrations (Fig. S6) range from a few hundreds of fg m^{-3} for selected rare earth elements (REEs), such as Er, Tm, Yb, and Lu, to tenths of μg m^{-3} for Na, spanning approximately seven orders of magnitude. This wide concentration range reflects both their environmental abundance and the characteristics of active sources in the vicinity of GAL. As expected, sea salt aerosol strongly influences the aerosol composition at Ny-Ålesund, consistent with previous findings (Conca et al., 2019; Zhan et al., 2017).

https://doi.org/10.5194/egusphere-2026-1467
Preprint. Discussion started: 9 April 2026

To identify the dominant source categories, namely crustal, marine, and anthropogenic, we calculated crustal (CEF, Fig. S8) and Marine (MEF, Fig. S9) enrichment factors, following Barberi et al. (2016). Elements with median CEF value < 10 and median MEF value > 10 were attributed to crustal sources, whereas those with median MEF value < 10 and median CEF value > 10 were attributed to marine sources. Elements for which both median CEF and MEF values exceeded 10 were classified as anthropogenic.

According to this classification, Cr, Ni, Cu, Pb, Mo, Zn, As, and Cd were associated with anthropogenic sources. These elements may originate from fossil fuel combustion, lubricants use, mining activities, and non-ferrous metal production (Kyllönen et al., 2020; Wong et al., 2021). The temporal variability normalized time series (Fig. S10d) display a strong seasonality, with elevated concentrations in winter and markedly lower in summer. This is typical for long-range transport of air pollution into the Arctic from lower latitudes, favoured by a stable tropospheric stratification, stronger winds, and the southward extension of the polar front in winter time (Platt et al., 2022; Stohl, 2006b).

Ni exhibited a distinct pattern, with an increase at the beginning of September followed by a gradual decline throughout the month. This anomaly is reflected in a low correlation with other elements. Although Ni is often associated with ship emissions, and typically highly correlated with V, the V/Ni ratio in September (0.3±0.2; mean±σ) was far lower than the typical range reported for ship emissions (2.5-4) (Becagli et al., 2020). In addition, the harbour traffic in Ny-Ålesund was relatively low in September 2022 (27 vessels, 991 passengers) compared to August (103 vessels; 3975 passengers) (Statistics – Kings Bay — Ny-Ålesund Harbour, 2025). Prevailing wind directions in September also do not support influence from the harbour to GAL (Fig. S11). Although Ni-V-Cr enrichment has been reported in soils of south-west Greenland, this potential source does not adequately explain the observed anomaly due to lack of coherent temporal variability among Ni, V, and Cr.

Concentrations of crustal elements (Figs. S10b and S10c) were generally higher in winter, when the surrounding terrain is snow-covered, indicating substantial influence from long-range transport. However, two notable crustal events occurred in summer, simultaneously with the increase of the concentration of sea salt elements. The first (17-23 August 2022) showed elevated concentrations of Sr and Mo, along with spikes of Na, Mg, Ca, and K (Fig. S10a). A second event occurred on 21-27 September 2022, but without similar enrichment of Sr and Mo, highlighting the distinct signature of the first event. Both events coincided with enhanced wind speed (Fig. S12), which likely promoted the resuspension of local soil and sea spray.

Higher concentrations of marine source elements in winter (Figure S10a) can be attributed to the higher burden of aerosol in the atmosphere by a combination of enhanced long-range transport from lower latitudes and weaker atmospheric removal processes (Spagnesi et al., 2025). Among the REE (Fig. S10c), Lu showed notable enrichment in early 2022 relative to other lanthanides, consistent with its higher CEF (Fig. S8) and higher correlation with anthropogenic elements (Figure S7). This enrichment may be related to refinery emissions at lower latitudes, where Lu serves as a catalyst in hydrocarbon processing (Nayebare et al., 2018). A statistically significant small positive correlation is present between Lu and V (Spearman's ρ correlation 0.48, p-value<0.05, H_0 -> ρ=0), an element typically associated with the combustion of fuel oils (Arienzo et al., 2021). The remaining REE follow concentration patterns previously reported for PM_{10} in the region (Conca et al., 2019). Ratios between light and heavy REEs (Pr/Yb = 0.9±0.5 and Pr/Er=1.4±0.9, mean±σ; normalized to upper crust continental values)

https://doi.org/10.5194/egusphere-2026-1467
Preprint. Discussion started: 9 April 2026

are close to unity, indicating little to no fractionation during transport. The Ce anomaly, averages 1.0±0.2 (mean±σ), suggesting no significant anthropogenic enrichment.

A comparison of selected elemental concentrations measured at GAL and at ZEP (Heavy metals at Zeppelin mountain (Ny-Ãlesund), 2025) shows generally higher values at ZEP, except from Pb and As, for which concentrations were similar at both sites. The differences between the elemental concentrations in the time series of GAL and ZEP are statistically significant with a Spearmen's ρ correlation that is different from zero just for Pb (0.46, p-value<0.05) and As (0.47, p-value<0.05). Samples from both observatories were digested using HNO_3, ensuring methodological consistency and facilitating direct comparison. However, the elemental data at ZEP refer to the fine fraction, whereas measurements at GAL were performed on PM_{10}. Consequently, the observed differences between the two sites reflect not only vertical gradients and meteorological influences, but also differences in the sampled size ranges. This implies that vertical contrasts in elemental concentrations may be even more pronounced than suggested by Table 2. Notably, this effect is most evident for crustal elements (Al, Fe, Ti, and Mn) and less so for anthropogenic species such as Pb and As.

Although both categories are predominantly influenced by long-range transport (Groot Zwaaftink et al., 2016), they exhibit distinctly different vertical behaviour, as anthropogenic species are mainly associated with the accumulation-mode, whereas crustal elements are mainly linked to coarser aerosol particles. This size-dependent vertical processing causes MD, even when present in the fine fraction, to be preferentially depleted during downward mixing towards the surface through deposition, whereas accumulation-mode particles remain well mixed. Consequently, air masses sampled at elevated sites such as ZEP are less affected by near-surface removal processes than those measured at GAL. These results indicate that the observed differences between the GAL and ZEP primarily reflect boundary-layer dynamics rather than differences in source origin, underscoring the key role of ABL in shaping the vertical distribution of aerosol in the Arctic atmosphere.

https://doi.org/10.5194/egusphere-2026-1467
Preprint. Discussion started: 9 April 2026

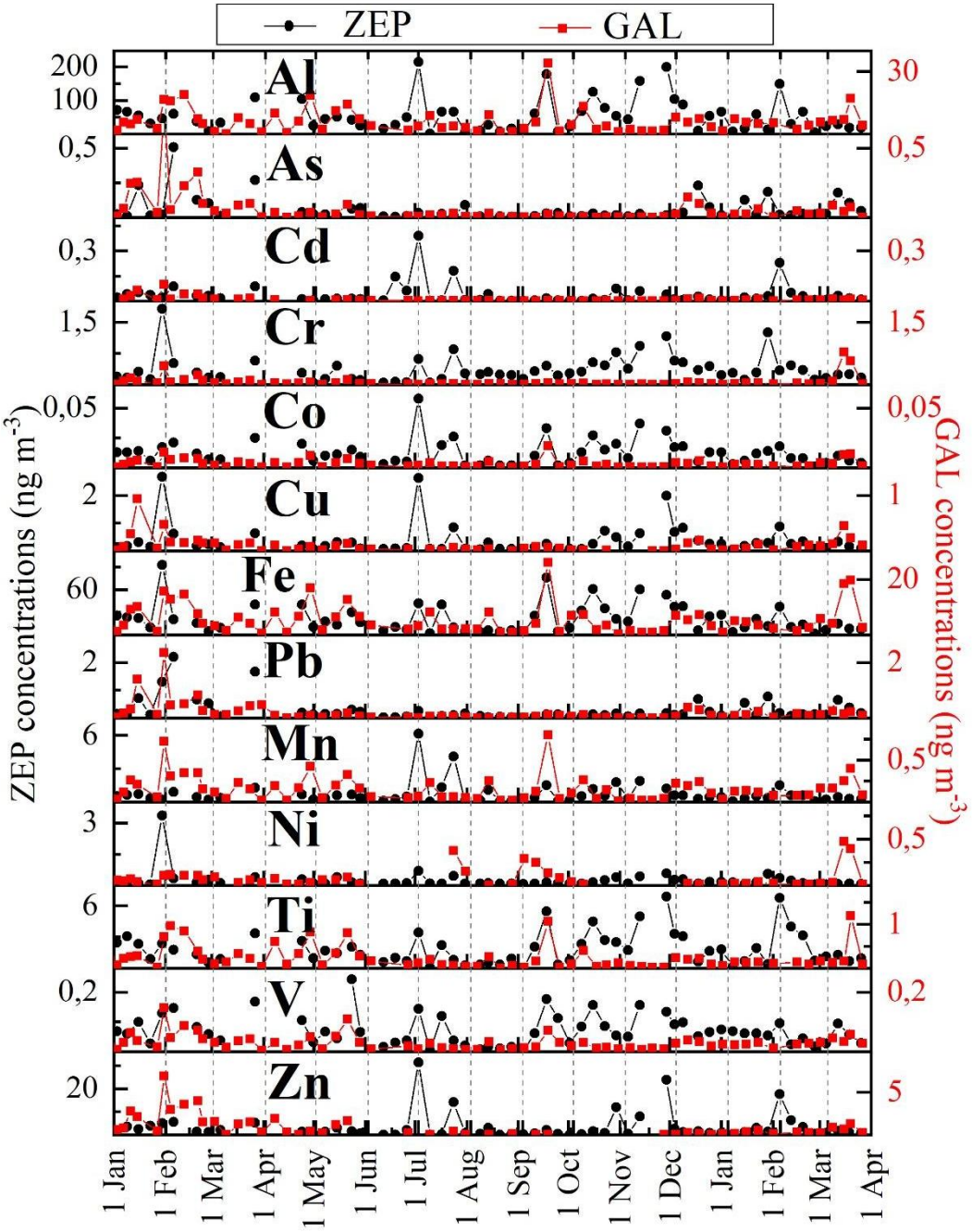

Figure 4. Comparison of the mass concentration in air for some elements between the samples collected at Gruvebadet atmosphere laboratory (this work, red line and dots) and at Zeppelin observatory ((Heavy metals at Zeppelin Mountain (Ny-Ålesund), 2025), black line and dots) for the period January 2022 to March 2023. The concentrations are reported in a logarithmic scale.

https://doi.org/10.5194/egusphere-2026-1467
Preprint. Discussion started: 9 April 2026

Table 2. Median and interquartile range for the season mass concentration for PM_{10} samples collected from January 2022 to March 2023 at Gruvebadet atmosphere laboratory and Zeppelin observatory (ng m^{-3}).

		Winter	Spring	Summer	Autumn
Al	GAL	5.4 (3.6)	6.1 (8.0)	3.3 (3.0)	2.2 (2.9)
	ZEP	53.1(50.3)	31.4(22.4)	21.7 (44.6)	64.3(95.5)
As	GAL	0.05 (0.11)	0.03 (0.06)	0.01 (0.01)	0.003 (0.004)
	ZEP	0.03 (0.11)	0.04 (0.05)	0.007 (0.012)	0.02 (0.02)
Cd	GAL	0.01 (0.02)	0.007 (0.006)	0.001 (0.001)	0.0006 (0.0002)
	ZEP	0.03 (0.03)	0.012 (0.007)	0.01 (0.08)	0.005 (0.019)
Cr	GAL	0.04 (0.06)	0.04 (0.07)	0.02 (0.01)	0.01 (0.01)
	ZEP	0.31 (0.27)	0.18 (0.12)	0.24 (0.22)	0.41 (0.30)
Co	GAL	0.003 (0.004)	0.004 (0.003)	0.001 (0.001)	0.001 (0.002)
	ZEP	0.013 (0.007)	0.010(0.006)	0.004(0.00725)	0.014(0.021)
Cu	GAL	0.09 (0.12)	0.1 (0.1)	0.03 (0.01)	0.02 (0.04)
	ZEP	0.26 (0.20)	0.17 (0.20)	0.07 (0.08)	0.21 (0.46)
Fe	GAL	4.3 (5.1)	5.8 (5.5)	2.1 (2.3)	1.6 (3.0)
	ZEP	20.3 (15.5)	14.1 (12.0)	6.1 (5.6)	28.7 (38.9)
Pb	GAL	0.16 (0.28)	0.12 (0.15)	0.03 (0.03)	0.01 (0.04)
	ZEP	0.16 (0.54)	0.19 (0.18)	0.05 (0.05)	0.11 (0.10)
Mn	GAL	0.13 (0.15)	0.12 (0.13)	0.06 (0.05)	0.04 (0.09)
	ZEP	0.46 (0.30)	0.38 (0.34)	0.20 (1.05)	0.54 (1.02)
Ni	GAL	0.03 (0.05)	0.03 (0.05)	0.01 (0.14)	0.11 (0.17)
	ZEP	0.15 (0.19)	0.09 (0.11)	0.09 (0.02)	0.12 (0.19)
Ti	GAL	0.19 (0.14)	0.15 (0.25)	0.08 (0.13)	0.06 (0.09)
	ZEP	1.83 (2.345)	1.29 (0.81)	0.64 (0.58)	2.42 (3.14)
V	GAL	0.03 (0.02)	0.03 (0.02)	0.01 (0.01)	0.01 (0.01)
	ZEP	0.07 (0.04)	0.06 (0.06)	0.02 (0.02)	0.09 (0.09)
Zn	GAL	0.5 (1.8)	0.6 (1.0)	0.1 (0.2)	0.07 (0.04)
	ZEP	1.6 (2.3)	1.4 (1.1)	0.4 (2.2)	0.8 (3.2)

3.5. Evaluation of natural and anthropogenic contributions using lead concentration, crustal enrichment, and isotopic composition

To better constrain the sources of PM_{10}, GAL samples were evaluated using Pb concentration, enrichment factors, and the $^{207}Pb/^{206}Pb$ and $^{208}Pb/^{206}Pb$ isotope ratios (Table S1).

https://doi.org/10.5194/egusphere-2026-1467
Preprint. Discussion started: 9 April 2026

Lead concentrations (mean: 174 pg m^{-3}; median: 80 pg m^{-3}) agree well with values reported for PM_{10} samples collected at GAL from 2018 to 2020 (mean: 143 pg m^{-3}; median: 55 pg m^{-3}) (Grotti et al., 2024). Likewise, the crustal enrichment factors (mean: 127; median 69) align with those previously reported (mean: 90; median 42) (Grotti et al., 2024), indicating a sustained influence of anthropogenic sources on atmospheric Pb at GAL.

The $^{208}Pb/^{206}Pb$ and $^{207}Pb/^{206}Pb$ isotope ratios agree well with those reported for PM_{10} samples collected at Ny-Ålesund during 2010 – 2020 (Bazzano et al., 2021; Grotti et al., 2024), and are similar to values observed at other High Arctic sites (Anon, 1989; Bory et al., 2014; Shotyk et al., 2005; Sturges et al., 1993).

Lead concentrations and CEFs exhibit the characteristic seasonal cycle for this region (Fig. S13), with higher values in samples collected from December to April (Pb concentration: 290 ± 362 pg m^{-3}; CEF:198 ± 187, n=30) than in those collected from May to November (Pb concentration: 50 ± 51 pg m^{-3}; CEF:52 ± 56, n=28). The difference between the two periods is statistically significant (Mann–Whitney test, $p < 0.001$).In contrast, the Pb isotope composition does not differ significantly between these two periods (Mann-Whitney test, $p > 0.6$): summer samples are characterized by isotope ratios (2.103 ± 0.012, 0.863 ± 0.008) that do not differ significantly from those in winter and spring (winter: 2.104 ± 0.007, 0.862 ± 0.002; spring: 2.105 ± 0.009, 0.861± 0.004). This feature was also observed in 2013 samples (Bazzano et al., 2016) and suggests a persistent influence of the same dominant Pb source during both winter/spring and summer. The observed isotopic composition is compatible with a Russian origin of atmospheric Pb at Ny-Ålesund (Ardini et al., 2020).

The relative natural and anthropogenic contributions to Pb the PM_{10} samples were assessed by calculating the corresponding end-members (EMs) following Grotti et al. (2024). Briefly, the isotopic data were grouped into six classes based on CEF (0–20, 20-35, 35-50, 50-100, 100-150, 150). Each Pb isotope ratio was then modelled as a linear function of 1/CEF, and the regression models were evaluated at CEF = 1 and CEF = ∞.

The estimated EMs (anthropogenic EM: $^{208}Pb/^{206}Pb = 2.108 \pm 0.001$, $^{207}Pb/^{206}Pb = 0.8633 \pm 0.0002$; natural EM: $^{208}Pb/^{206}Pb = 1.906 \pm 0.025$, $^{207}Pb/^{206}Pb = 0.744 \pm 0.007$) are represented in a three-isotope plot along with the Pb isotopic compositions of the PM_{10} samples (monthly-averages) and some reference values from literature (Fig. 5). The mixing line between the anthropogenic and natural end-members stretches towards the isotopic composition of the upper continental crust (UCC) (Asmerom and Jacobsen, 1993) and passes through the area of Pb isotope ratio values of sediments collected in the Kongsfjorden and at Ny-Ålesund (Bazzano et al., 2014). This finding suggests that the natural input to atmospheric Pb in this area is most likely due to crustal material. However, given the Euclidean distances of the Pb isotope ratios of the samples from the calculated EM signatures, the relative contribution of the natural origin appears to be negligible.

The $^{208}Pb/^{206}Pb$ and $^{207}Pb/^{206}Pb$ ratios of the anthropogenic EM are in good agreement with previous estimations (2.107 ± 0.002 and 0.864 ± 0.001) (Grotti et al., 2024) and compatible with the isotopic signature of Pb ores from the main mining sites for Pb in East Kazakhstan and the Altai region (Zyranovsk: $^{208}Pb/^{206}Pb = 2.099$, $^{207}Pb/^{206}Pb = 0.865$ and Leninogorsk (now Ridder): $^{208}Pb/^{206}Pb = 2.098$, $^{207}Pb/^{206}Pb = 0.867$) (Mukai et al., 2001). Since the majority of the Pb measured in the considered PM_{10} samples is anthropogenic, this area can be identified as one of the main sources of this element at Ny-Ålesund. On the other

https://doi.org/10.5194/egusphere-2026-1467
Preprint. Discussion started: 9 April 2026

hand, emissions from Kola Peninsula smelters can be disregarded, as they appear to have low isotope ratios (Sturges and Barrie, 1989).

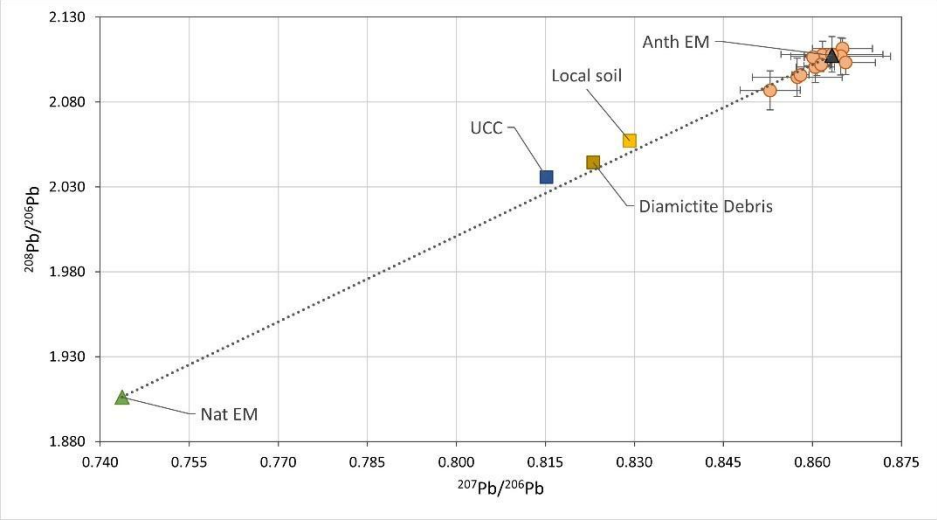

Fig. 5. Three-isotope plots $^{208}Pb/^{206}Pb$ vs $^{207}Pb/^{206}Pb$. Circles represent monthly averaged Pb isotope ratios in PM_{10} samples collected at Ny-Ålesund from February 2022 to March 2023.

3.6. Dust aerosol component

Mineral dust (MD) concentrations were determined using four approaches, each based on the chemical composition of the collected aerosol, as described below:

1. Crustal oxides (Na_2O, MgO, SiO_2, Al_2O_3, TiO_2, K_2O, CaO, Fe_2O_3): MD concentration were estimated as the sum of the oxide-equivalent masses of major crustal elements (Na, Mg, Si, Al, Ti, K, Ca, and Fe). Elemental concentrations were converted to oxide weights using stoichiometric multipliers based on the crustal composition profile reported by Henderson and Henderson (2009).

$$\text{Mineral dust} = 1.35[Na] + 1.66[Mg] + 1.89[Al] + 2.14[Si] + 1.21[K] + 1.40[Ca] + 1.67[Ti] + 1.43[Fe]$$

2. Anthropogenically corrected oxide summation: This approach refines Method 1 by accounting for potential non-crustal (anthropogenic) contributions of K, Ca, and Fe. The crustal fractions of these elements are estimated from the measured aluminum (Al) concentration using the crustal element-to-Al ratios reported by Henderson and Henderson (2009).

$$\text{Dust} = 1.35[Na] + 1.66[Mg] + 3.79[Al] + 2.14[Si] + 1.67[Ti]$$

3. Sea-Salt and anthropogenically corrected oxide summation: This method extends Method 2 by additionally accounting for the sea salt contribution to sodium (Na) and magnesium (Mg). Non-sea-salt concentrations (nssNa and nssMg) were calculated as follows:

$$\text{Dust} = 1.35[nssNa] + 1.66[nssMg] + 1.89[Al] + 2.14[Si] + 1.21[K] + 1.40[Ca] + 1.67[Ti] + 1.43[Fe]$$

https://doi.org/10.5194/egusphere-2026-1467
Preprint. Discussion started: 9 April 2026

where

$$[nssNa] = 0.35[Al] \text{ and } [nssMg] = [Mg] - [ssMg] = [Mg] - 0.12[ssNa] = [Mg] - 0.12([Na]-[nssNa])$$

4. Aluminum-Based "Rule of Thumb": This simplified approach estimates mineral dust from the measured aluminium concentration, using aluminum's average mass fraction in the upper continental crust to provide a rapid proxy for dust concentration.

A comparison of the results from the four approaches is presented in Figure 6. The first two methods show a notable agreement, which suggests that the yearly average anthropogenic contributions of elements like K, Ca, and Fe are negligible compared to the dust's crustal contribution. However, these two methods consistently overestimate dust concentration relative to the other two approaches, which also show a reasonable agreement with each other.

Method 3, which corrects for both sea-salt and anthropogenic contributions, was ultimately selected as the most reliable approach for this study. Given the sampling site's location in Ny-Ålesund, a coastal environment within a fjord, the contribution of sea spray to Na and Mg concentrations is expected to be significant. Therefore, explicitly accounting for these sea-salt contributions provides a more accurate representation of the true crustal dust component. This exercise highlights the importance of selecting a methodology that is appropriate for the specific environmental context of the sampling location.

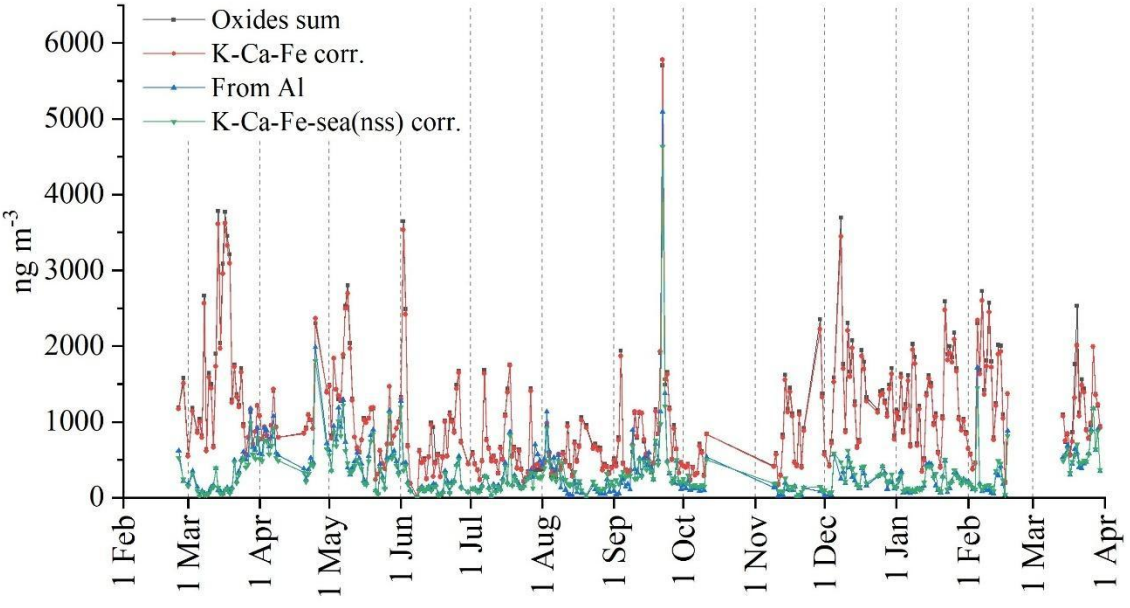

Fig. 6. Dust concentration as obtained following the approaches described in paragraph 3.5; i.e. as an oxides sum (appr. 1), K-Ca-Fe corr. (appr. 2), K-Ca-Fe sea(nss) corr. (appr. 3), or finally form the sole Al assessment following the approach 4.

https://doi.org/10.5194/egusphere-2026-1467
Preprint. Discussion started: 9 April 2026

Analysis of the CEFs for crustal elements showed that the CEF of Silicon remained consistently close to 1 throughout the year. This suggests a stable silicon-to-aluminium ratio in the dust source. A notable exception occurred in August 2022, when elevated CEFs were observed for multiple elements. Back-trajectory analysis for this period shows air masses traveling along an Iceland-Greenland-Canada pathway where potential dust sources might be located (see Figure S17, right panel); however, the back-trajectory analysis cannot rule out local sources.

Aluminium concentration has proven to be a reliable proxy for aerosol dust in Ny-Ålesund. Comparing Al concentration data from two different sites (GAL and ZEP) can help differentiate between dust transport processes occurring above the Arctic Boundary Layer and local dust resuspension events.

Figure 7 shows the Al concentration measured at both GAL and ZEP, with GAL data providing a higher temporal resolution. A significant difference in the temporal trends was observed at the beginning of July 2022. During this time, Al concentrations at ZEP were considerably higher than at GAL. This discrepancy suggests a dust transport event at a higher altitude, with the elevated concentrations observed at the ZEP station not reaching the lower-lying GAL station.

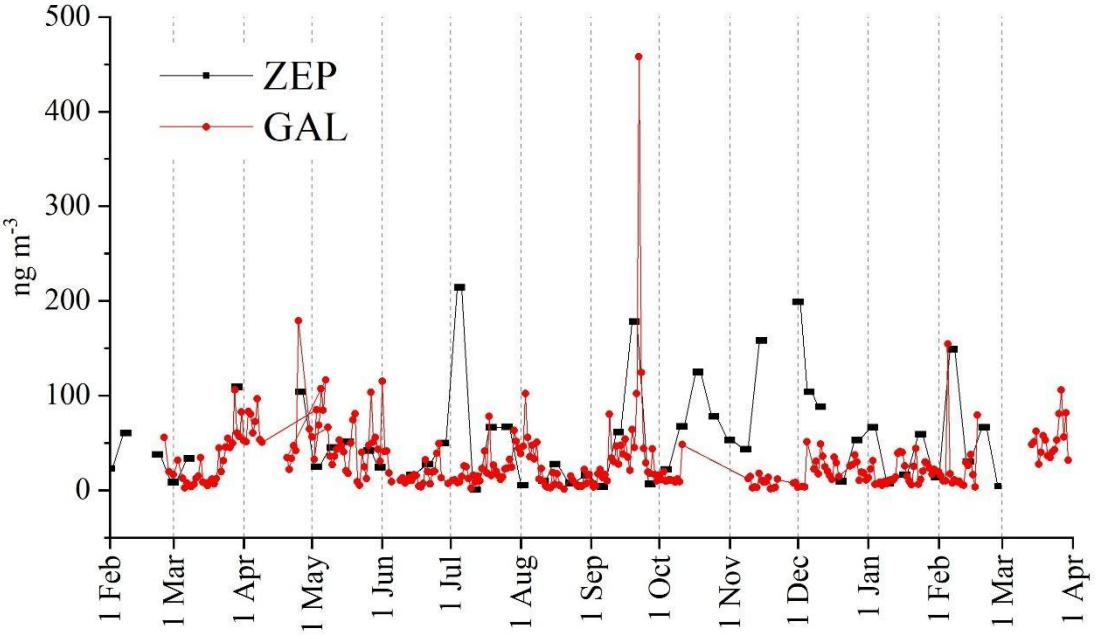

Fig. 7. Aluminium concentrations measured at both GVB and ZEP

The monthly average aerosol mass (Fig. S15), measured gravimetrically on filters before PIXE analysis, was compared with a reconstructed mass based on PIXE and Thermo-Optical Analysis data. The difference between these two values, defined as

https://doi.org/10.5194/egusphere-2026-1467
Preprint. Discussion started: 9 April 2026

"unexplained mass", is primarily attributed to ionic components such as nitrates, which were not directly measured. While sulfates were estimated based on the measured sulfur (S) concentration, other ionic species were not accounted for.

A clear seasonal pattern was observed in the PM loadings (Fig. S15). Concentrations were lower during the summer and autumn months and higher during winter and spring. Similarly, dust contributions were at their minimum during the summer.

3.7. Carbonaceous components

Organic carbon (OC), elemental carbon (EC), and total carbon (TC) have been measured at GAL since 2011 (Caiazzo et al., 2021) and at ZEP since 2017 (Yttri et al., 2021). The main differences compared to the ZEP protocol concern the sampling duration (see Table 1) and the thermal protocol used for the thermo-optical analysis; at GAL, analyses have been performed using the NIOSH-870 protocol).

Within the framework of this project, sampling and analytical procedures at GAL and ZEP were harmonized for a one-year period (Table 1). During this period, OC and EC were analyzed on PM_{10} filter samples using the EUSAAR_2 thermal protocol (Cavalli et al., 2010).

For a shorter overlapping period, GAL data obtained according to the procedure reported by Caiazzo et al. (2021) were compared with GAL data generated using the standardized procedure to assess the comparability of the two data series (with the purpose to avoid abrupt changes in the GAL data series). The results show a reasonable agreement between the two datasets (Fig. 8), having different time resolution (4 and 7 days respectively), with monthly OC averages differing by approximately 10% (range: 4-17%). The comparison of EC data is more uncertain: besides the difficulty of comparing data for samples collected with different time resolution, concentrations are frequently below the detection limit. These findings suggest that the two thermal protocols (EUSAAR_2 and NIOSH-870) may produce comparable results for Arctic aerosol, although further work focused on thermal protocols is needed..

GAL data for the observation period fall within the range previously observed (Caiazzo et al., 2021), although some lower values were observed. Notably, these measurements are among the first obtained while the GAL observatory operated during the Polar Night (October-February). Lower OC concentrations during winter may reflect reduced biogenic activity, more extensive sea-ice coverage, decreased long-range transport from anthropogenic source regions, and a lower frequency of fire events.

Comparing GAL and ZEP, the two observatories exhibit similar temporal behaviour for both OC and EC, although concentrations are slightly lower at ZEP. This suggests that both sites are influenced by long-range transport of carbonaceous aerosol, while GAL appears to possibly experience an additional contribution from local or regional sources, as futher suggested by the results shown in Fig.11 (see later).

https://doi.org/10.5194/egusphere-2026-1467
Preprint. Discussion started: 9 April 2026

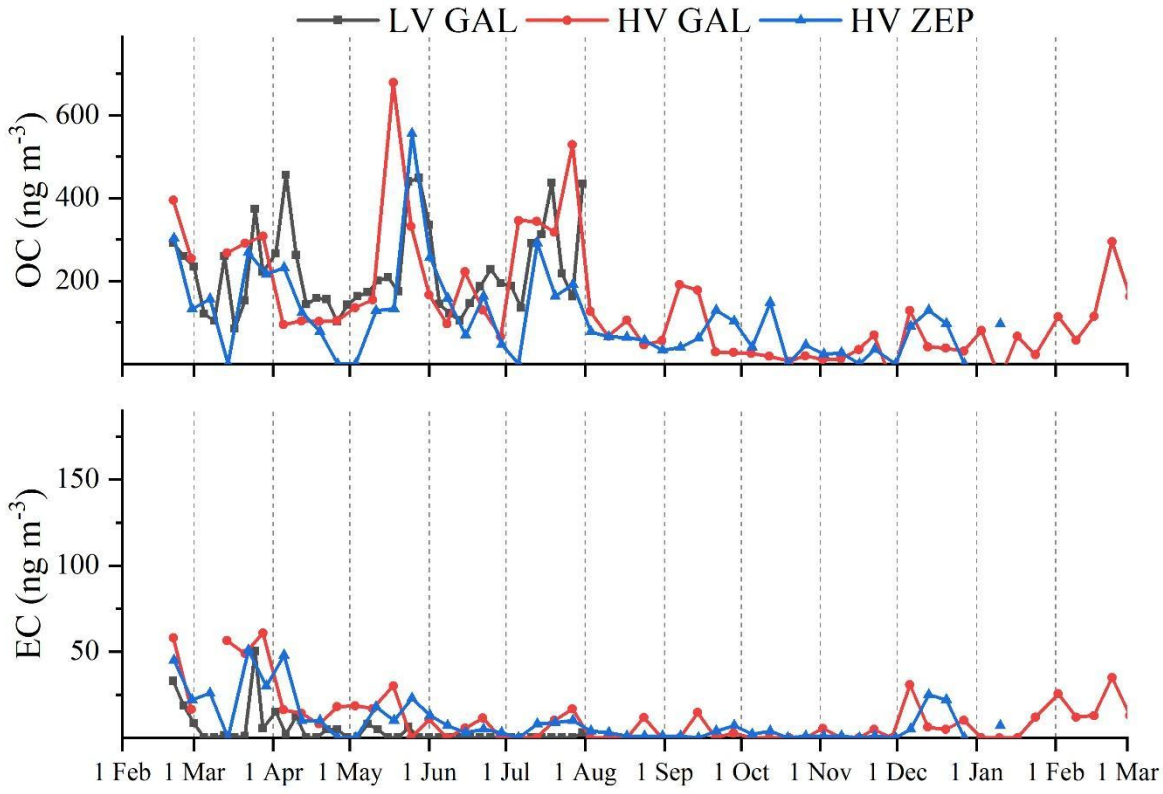

Fig. 8. OC (upper panel) and EC (lower panel) concentrations measured at both ZEP and GAL. ZEP results are obtained from a HV sampler (7 days, EUSAAR2), while for GAL results as obtained from the HV sampler (7 days, EUSAAR2) harmonized with ZEP and from the LV sampler (4 day-resolution, NIOSH-870) used in the past.

3.8. Biomass burning and biogenic organic tracers

Figure 9 shows concentrations of the biomass-burning tracers levoglucosan, mannosan, and galactosan (Simoneit, 1999), the fungal spore tracers arabitol and mannitol (Bauer et al., 2008), and the more generalized PBAP tracers glucose and fructose measured at GAL and ZEP during BETHA-NyÅ. To verify laboratory performance comparability, four samples collected in spring and summer at ZEP were additionally analyzed at the Venice Lab. No statistically significant differences were found for any of the species between the Venice and NILU analyses (Wilcoxon test, $p > 0.05$; Fig. S16).

https://doi.org/10.5194/egusphere-2026-1467
Preprint. Discussion started: 9 April 2026

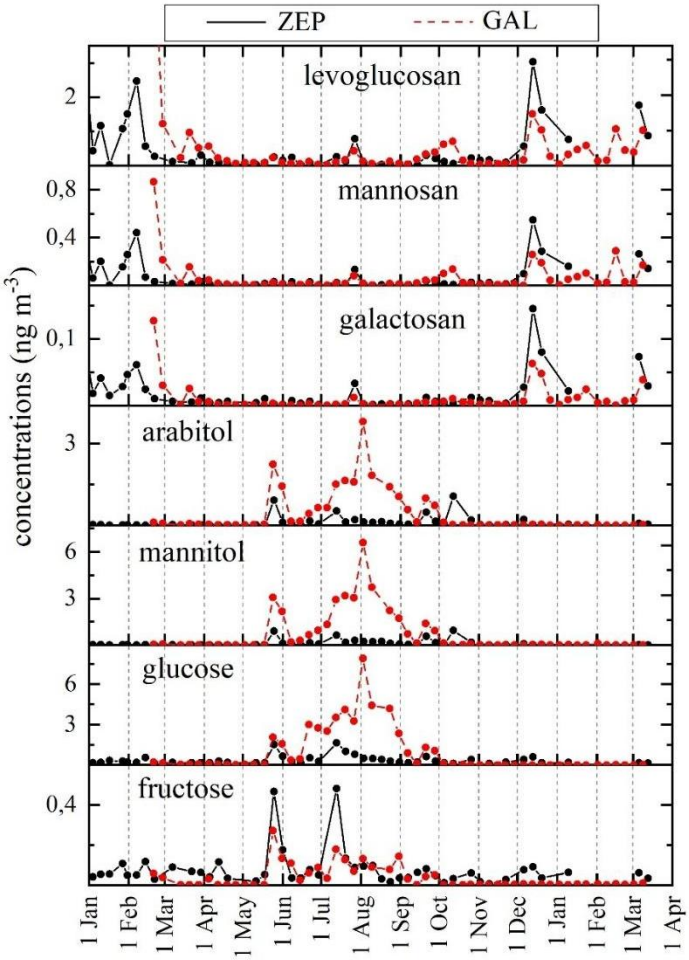

Fig. 9. Levels of biomass burning tracers (levoglucosan, mannosan, and galactosan) and PBAP markers (arabitol, mannitol, glucose, and fructose) at GAL and ZEP from Jan 2022 to Apr 2023.

The different tracers exhibit distinct behaviors. Arabitol and mannitol show pronounced summer maxima at GAL, whereas no comparable enhancement is observed at ZEP. These compounds are primarily associated with the coarse aerosol fraction (> 1 µm) (Feltracco et al., 2020) and indicate a local input from fungal spores near ground level. Due to their relatively large particle size, these particles are less efficiently transported upward within the mixing layer, which may explain the lower levels observed at the higher-altitude ZEP observatory.

Glucose is a less source-specific tracer, as it may originate from both biomass burning and PBAP sources (Feltracco et al., 2020). In this case, however, glucose follows the same pattern as the fungal spore tracers (Fig. 9), indicating a predominantly

https://doi.org/10.5194/egusphere-2026-1467
Preprint. Discussion started: 9 April 2026

biogenic origin. In contrast, fructose exhibits a different temporal behavior, although some peaks coincide with those of glucose.

The observed levoglucosan concentrations are largely driven by long-range transport of emissions from residential wood combustion (RWC) and wildfires, although contributions from local sources cannot be excluded. The isolated peak observed at GAL at the beginning of the BETHA-NyÅ campaign is likely attributable to a local source. In contrast, the recurrent peaks observed at ZEP during the heating season (Nov-Apr) are consistent with RWC, as previously demonstrated by Yttri et al. (2024).

Not all levoglucosan maxima correspond to documented wildfires or RWC activity. Nevertheless, the relatively high concentrations observed during the second half of March and the first half of April may be linked to events in central and eastern Europe as well as in central Asia (see Fig. S17). Similarly, the slight increase in concentrations in late July and early August may be associated with events in Europe, northern Asia, and North America (see Fig. S18). Comparable interpretations apply to the maximum in early October 2022 (left panel of Fig. S19) and to one of the highest peaks detected in mid-December. Elevated concentrations measured in early 2023 were likely influenced by fires primarily located in central and eastern Europe (right panel of Fig. S19).

Owing to the relatively long sampling intervals and rapidly changing circulation patterns, the fire source influencing the observed concentrations often extend over large geographical areas.

The isomeric ratio of levoglucosan to mannosan, proposed as a diagnostic indicator of the type of burned vegetation (Fabbri et al., 2009), does not differ significantly between GAL (8±4) and ZEP (8±3). Although Yttri et al. (2024) reported differences between the heating (Nov-May) and non-heating (Jun-Oct) periods at ZEP for 2017-2020, no such difference is observed for the period considered here: the levoglucosan/mannosan ratios are 8±4 (GAL) and 7±1 (ZEP) during the heating season (7.5±1.9 for Yttri et al. (2024)), and 8±4 (GAL) and 8±5 (ZEP) during the non-heating season (4.8±1.2 for Yttri et al. (2024)). Given that levoglucosan/mannosan ratios are typically higher for hardwood combustion (14–15) and lower (3–5) for softwood combustion (Schmidl et al., 2008), the values observed at both sites suggest a mixture of hardwood and softwood combustion, consistent with previous findings from the region (Feltracco et al., 2020).

3.9. Analysis of difference between GAL and ZEP and its main drivers

We used multivariate statistical analysis to quantify the compound-specific differences between GAL and ZEP, highlighted in the preceding sections. Preliminary analysis with the Shapiro-Wilk test demonstrated that the data were not normally distributed and for this reason Linear Discriminant Analysis (LDA) was excluded as a chemometric approach. Instead, the Kruskal-Wallis test confirmed significant site-related differences in the measured chemical variables, whereas Partial Least Squares Discriminant Analysis (PLS-DA) was used to identify the species most responsible for discriminating between the two sites.

https://doi.org/10.5194/egusphere-2026-1467
Preprint. Discussion started: 9 April 2026

The input matrix consisted of 30 chemical species and 106 observations, corresponding to 53 weekly samples simultaneously collected at GAL and ZEP. A large fraction of the variance was explained by the first two latent factors (Fig. S20 and Table S2), accounting for 38% and 61% of the cumulative variance in the predictor (X) and response (Y, sites classification). The high proportion of explained Y variance indicates that the chemical differences between two sites are statistically significant. The PLS-DA coefficient plot displays the estimated regression coefficients for each variable, providing insight into both the direction and magnitude of their contribution to site discrimination (Fig. 10A). The anthropogenic species Cd, Cr, and V are the most influential variables associated with GAL. In contrast, As, Co, Cu, Pb, Mn, and Ni emerge as the most relevant variables for ZEP, together with arabitol and mannitol.

The Variable Importance in Projection (VIP) plot (Fig. 10B), interpreted in conjunction with the coefficient plot, summarizes the overall contribution of each variable to the PLS-DA model. While the coefficient plot highlights the direction and magnitude of individual effects, the VIP plot ranks variables according to their global relevance, thereby facilitating interpretation. The VIP analysis indicates that ionic species play a substantial role in differentiating the two sites, with Na and K showing particularly high importance.

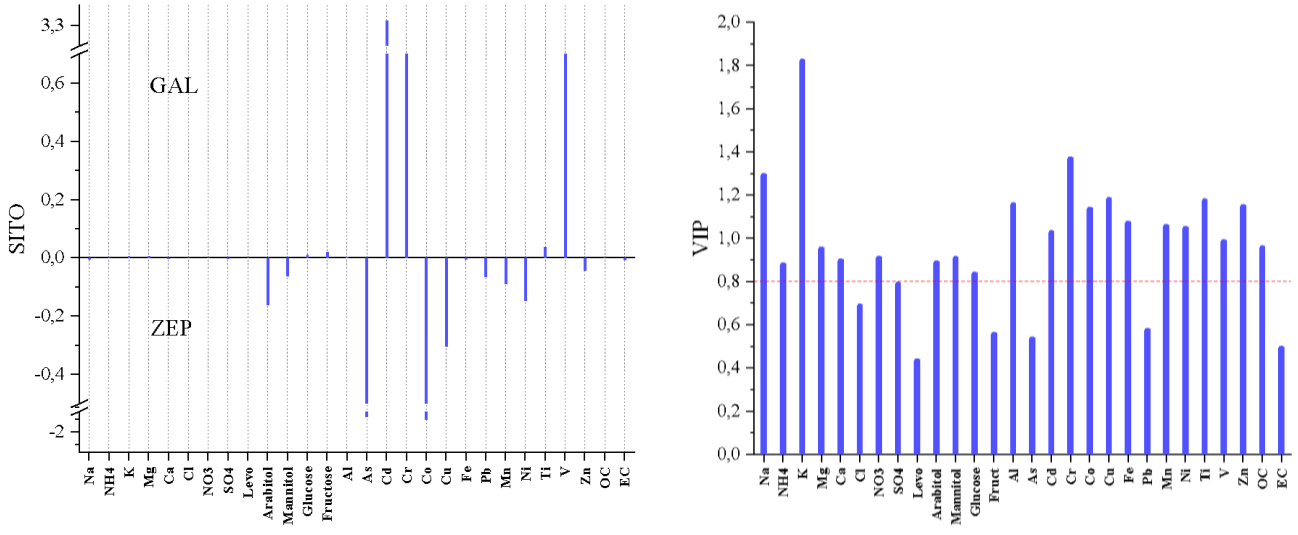

Fig. 10. A) Coefficients plot and B) Variable Importance in Projection (VIP) plot obtained with PLS-DA, explained which compound impacts on the difference of each site.

https://doi.org/10.5194/egusphere-2026-1467
Preprint. Discussion started: 9 April 2026

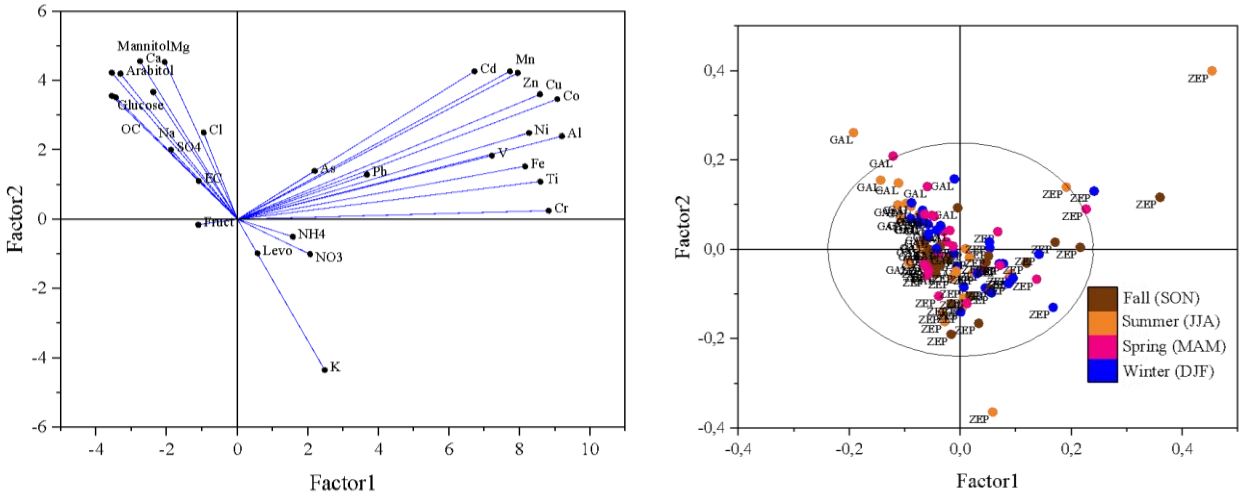

Fig. 11. A) Factor loading and B) scores loading obtained with PLS-DA.

The loading plot (Fig. 11A) illustrates how variables contribute to the latent components and identifies the chemical species most responsible for class separation. Factor 1 is associated with trace metals of predominantly anthropogenic (e.g., Cd, Co, Cu, Pb, As) and crustal origin. Factor 2 is primarily driven by markers of PBAP, such as arabitol, mannitol, and glucose, together with sea salt aerosol (Na^+ and Cl^-), combustion-related aerosol (e.g., EC) and the ubiquitous OC. The clustering of levoglucosan, K^+, NH_4^+, and NO_3^- reflects a mixed influence of biomass-burning emissions and secondary inorganic aerosol (NH_4^+ and NO_3^-) formation.

The score plot (Fig. 11B) shows the distribution of samples across seasons. In general, samples cluster close to the origin, indicating substantial overlap between sites and season and suggesting broadly similar chemical composition. Nevertheless, several samples deviate from the main cluster, pointing to episodic source influences. Some GAL samples collected during summer and spring show positive shifts along Factor 2, consistent with enhanced contributions from biogenic sources during the growing season. Conversely, isolated ZEP samples are shifted along Factor 1, likely reflecting episodes of long-range transport of anthropogenic aerosols.

Overall, the PLS-DA results indicate that, despite substantial overlap in chemical composition, seasonal variability is driven by a limited set of source-related variables. Biogenic species dominate the summer variability, whereas anthropogenic species contribute more consistently throughout the year at both sites. This indicates that PLS-DA captures subtle, yet systematic, differences in source influences across sites and seasons.

The Arctic boundary layer (ABL) is typically shallow (<200 m), stably stratified, and often capped by low clouds, although its depth varies strongly with season and surface type. Over continental regions, ABL deepens during summer (up to > 1.5 km), whereas over oceanic areas it is thickest in winter and spring due to strong air–sea temperature contrasts (Esau and

https://doi.org/10.5194/egusphere-2026-1467
Preprint. Discussion started: 9 April 2026

Sorokina, 2009). During summer, GAL and ZEP are therefore expected to experience similar air masses with broadly similar chemical composition; however, local near-surface sources can still introduce differences between the two sites. In particular, arabitol and mannitol, tracers of fungal spores, are emitted close to ground level and are mainly associated with coarse particles (Feltracco et al., 2020). As ZEP is located well above these sources, such species are less likely to reach its altitude, explaining the lower concentrations observed at ZEP.

During winter, stronger stratification and a shallower ABL enhance vertical gradients. This is clearly reflected in the score plot (Fig. 11B), where winter samples (blue symbols) from GAL and ZEP are distinctly separated from one another along Factor 1. While ZEP shows a stronger influence of biomass burning species, consistent with its greater sensitivity to the long-range transport of polluted air masses, GAL appears more influenced by SSA. This signature in GAL could be linked to an increased frequency of regional cyclonic systems (Huang and Jaeglé, 2017) or, potentially, to local emissions originating from the fjord.

4 Conclusions

The BETHA-NyÅ project successfully demonstrated the feasibility and scientific value of coordinated aerosol measurements at different altitudes in Ny-Ålesund. The coordinated effort between the GAL and ZEP observatories, combined with meteorological observations from the Amundsen-Nobile Climate Change Tower, enabled a characterization of Ny-Ålesund vertical distribution on aerosol composition.

The study achieved a high degree of seasonal coherence between the two sites, particularly for anthropogenic markers associated with the Arctic Haze phenomenon. Sulphate and ammonium concentrations exhibited nearly identical temporal trends, with sulphate levels peaking in March-April at both locations. Quantitatively, median sulphate concentrations were remarkably consistent, recorded at 203 ng m^{-3} at GAL and 220 ng m^{-3} at Zeppelin. Optical properties also showed alignment during the cold season (November to April), with median scattering coefficients of 5.5 Mm^{-1} at ZEP and 4.2 Mm^{-1} at GAL. These results confirm that long-range transport of polluted air masses often overcomes local vertical gradients, resulting in a well-mixed lower atmosphere during haze episodes.

The harmonization protocol proved robust, revealing that while long-range signals are uniform, local differences emerge due to near-surface sources and boundary layer dynamics. The most significant site-specific variations were observed for biogenic tracers like arabitol and mannitol, which showed higher concentrations at GAL. This suggests that primary biological aerosol particles (PBAPs) are predominantly emitted from local terrestrial or marine sources near sea level and are trapped within a shallow, stable ABL, often failing to reach the elevation of the Zeppelin observatory.

Our findings on lead (Pb) concentrations (mean: 174 pg m^{-3}) at GAL align with previous long-term monitoring efforts (2010–2020), indicating a stable and persistent anthropogenic influence. Lead isotopic ratios ($^{208}Pb/^{206}Pb$ ~2.10 and $^{207}Pb/^{206}Pb$ ~0.86) remain consistent with Eurasian and Russian sources, confirming that the transport pathways for heavy metals into the Svalbard region have not significantly shifted in the last decade.

https://doi.org/10.5194/egusphere-2026-1467
Preprint. Discussion started: 9 April 2026

These results have direct implications for our understanding of Arctic Amplification. The persistent presence of Eurasian anthropogenic aerosols and the stratification of biogenic particles influence the region's radiative balance and cloud formation processes. Specifically, the trapping of aerosols within a shallow ABL can enhance local warming through surface-atmosphere interactions. This study reinforces the necessity of integrated, multi-altitude monitoring networks to accurately model the deposition of pollutants on snow and ice, a critical driver of the ice-albedo feedback mechanism in a rapidly changing Arctic environment.

Data availability

Data about GAL measurements are available at IADC (DOI to be assigned). All data from ZEP are open access and are available at http://ebas.nilu.no/. Different ZEP measurements are reported in different database (https://doi.org/10.48597/R38F-6XPS; https://doi.org/10.48597/ECGE-V26Y; https://doi.org/10.48597/6PXH-3ESD).

Competing interests

At least one of the (co-)authors is a member of the editorial board of Atmospheric Chemistry and Physics.

Author contributions

EB: Conceptualization, Data curation, Funding acquisition, Investigation, Methodology, Project administration, Supervision, Writing (original draft preparation); FA: Data curation, Investigation, Methodology, Writing (original draft preparation); SB: Conceptualization, Data curation, Investigation, Methodology, Writing (original draft preparation); SB: Data curation, Investigation, Methodology, Writing (original draft preparation); FB: Data curation, Investigation, Writing (review and editing); GC: Conceptualization, Data curation, Investigation, Methodology, Writing (original draft preparation); AC: Data curation, Writing (review and editing); DC: Conceptualization, Data curation, Investigation, Methodology, Writing (original draft preparation); SC: Data curation, Investigation, Methodology, Writing (original draft preparation); MF: Data curation, Investigation, Methodology, Writing (original draft preparation); AG: Writing (review and editing), Supervision; FG: Data curation, Investigation, Methodology, Writing (review and editing); SG: Conceptualization, Data curation, Investigation, Methodology, Writing (original draft preparation); MG: Data curation, Investigation, Methodology, Writing (review and editing); DHR: Investigation, Methodology, Writing (review and editing); RK: Data curation, Investigation, Methodology, Writing (review and editing); MM: Data curation, Investigation, Methodology, Writing (original draft preparation), Supervision; MM: Investigation, Writing (review and editing); SM: Investigation, Writing (review and editing); SN: Investigation, Writing (review and editing); MP: Investigation, Writing (review and editing); MR: Investigation, Writing

https://doi.org/10.5194/egusphere-2026-1467
Preprint. Discussion started: 9 April 2026

(review and editing); CR: Data curation, Writing (review and editing); MS: Data curation, Investigation, Methodology, Writing (review and editing); AS: Data curation, Investigation, Methodology, Writing (review and editing); RT: Conceptualization, Data curation, Investigation, Methodology, Writing (original draft preparation); HU: Investigation, Methodology, Writing (review and editing); GV: Data curation, Writing (review and editing); TV: Investigation, Writing (review and editing); KEY: Data curation, Investigation, Methodology, Writing (review and editing); WA. Data curation, Investigation, Methodology, Writing (review and editing); MM: Conceptualization, Data curation, Investigation, Methodology, Writing (original draft preparation).

Funding

This research was funded by the Italian Ministry of University and Research (MUR) within the framework of the Arctic Research Program of Italy of the project ‘‘BETHA-NyÅ’’ - Boundary layer evolution through harmonization of aerosol measurements at Ny-Ålesund research station (PRA2021-0020). The Stockholm University observations were financially supported by the Swedish Environmental Protection Agency (Naturvårdsverket) and by ACTRIS-Sweden. The measurements of inorganic ions and trace elements at Zeppelin were funded by the Norwegian Environmental Agency while organic tracers were financed by the Norwegian Ministry of Climate and Environment.

Acknowledgments

The authors would like to dedicate this paper to the memory of our late colleague, Dr. Angelo Viola, who contributed significantly to the creation and operation of the Gruvebadet Atmospheric Laboratory. BETHA-NyÅ was his last project.
The scientific activity in Ny-Ålesund was carried out in the framework of the National Research Council of Italy (CNR) polar program. Logistical support of the CNR-Institute of Polar Sciences (CNR-ISP) is gratefully acknowledged. We want to thank all colleagues at the CNR Dirigibile Italia Arctic Station who worked during the field campaign. This paper is part of a collaborative effort carried out within the activities of Working Group 4 ‘Aerosols in Polar and Remote Areas’ of the Italian Aerosol Society (IAS).
The authors gratefully acknowledge the NOAA Air Resources Laboratory (ARL) for the provision of the HYSPLIT transport and dispersion model and READY website (http://www.ready.noaa.gov) used in this publication.
We acknowledge the help of ELGA LabWater in providing the PURELAB Pulse and PURELAB Flex. The authors are thankful to Norwegian Polar Institute (NPI) for support and management of observations at Zeppelin station.

https://doi.org/10.5194/egusphere-2026-1467
Preprint. Discussion started: 9 April 2026

References

Aas, W., Eckhardt, S., Evangeliou, Nikolaos, Duflot, V., Hjellbrekke, A., Platt, S. M., Solberg, S., and Yttri, K. E.: Monitoring of long-range transported air pollutants in Norway. Annual Report 2024, NILU, 2025.

Ardini F, Bazzano A, Grotti M.: Lead isotopic ratios in the Arctic environment. Environmental Chemistry 17, 213–239. https://doi.org/10.1071/EN19227, 2020.

Arienzo, M. M., Legrand, M., Preunkert, S., Stohl, A., Chellman, N., Eckhardt, S., et al. (2021). Alpine ice-core evidence of a large increase in vanadium and molybdenum pollution in Western Europe during the 20th century. Journal of Geophysical Research: Atmospheres, 126, e2020JD033211. https://doi.org/10.1029/2020JD033211

Heavy metals at Zeppelin mountain (Ny-Ãlesund): https://thredds.nilu.no/thredds/dodsC/ebas/NO0042G.20170102070000.20240701135921.high_vol_sampler..aerosol.7y.1w.NO01L_NILU_hvs_2d_0042.NO01L_icp_ms.lev2.nc, last access: 24 January 2025.

Anderson, T. L. and Ogren, J. A.: Determining Aerosol Radiative Properties Using the TSI 3563 Integrating Nephelometer, Aerosol Science and Technology, 29, 57–69, https://doi.org/10.1080/02786829808965551, 1998.

Anon: Stable lead isotope ratios in arctic aerosols: evidence for the origin of arctic air pollution, Atmospheric Environment (1967), 23, 2513–2519, https://doi.org/10.1016/0004-6981(89)90263-1, 1989.

NASA-FIRMS: https://firms.modaps.eosdis.nasa.gov/map/, last access: 4 August 2025.

Statistics – Kings Bay — Ny-Ålesund Harbour: https://port.kingsbay.no/statistics/?portyear=2022, last access: 21 January 2025.

Asmerom, Y. and Jacobsen, S. B.: The Pb isotopic evolution of the Earth: inferences from river water suspended loads, Earth and Planetary Science Letters, 115, 245–256, https://doi.org/10.1016/0012-821X(93)90225-X, 1993.

Asmi, E., Backman, J., Servomaa, H., Virkkula, A., Gini, M. I., Eleftheriadis, K., Müller, T., Ohata, S., Kondo, Y., and Hyvärinen, A.: Absorption instruments inter-comparison campaign at the Arctic Pallas station, Atmos. Meas. Tech., 14, 5397–5413, https://doi.org/10.5194/amt-14-5397-2021, 2021.

Barbaro, E., Kirchgeorg, T., Zangrando, R., Vecchiato, M., Piazza, R., Barbante, C., and Gambaro, A.: Sugars in Antarctic aerosol, Atmospheric Environment, 118, 135–144, https://doi.org/10.1016/j.atmosenv.2015.07.047, 2015.

Barbaro, E., Feltracco, M., Ulgelmo, B., Spagnesi, A., Frassati, S., Mazzi, G., Spolaor, A., Barbante, C., and Gambaro, A.: First evidence of benzothiazoles in arctic aerosols: Seasonal trend and sources attribution, Science of The Total Environment, 957, 177722, https://doi.org/10.1016/j.scitotenv.2024.177722, 2024.

Barbieri, M.: The Importance of Enrichment Factor (EF) and Geoaccumulation Index (Igeo) to Evaluate the Soil Contamination, Journal of Geology & Geophysics, 5, 1–4, https://doi.org/10.4172/2381-8719.1000237, 2016.

Bauer, H., Claeys, M., Vermeylen, R., Schueller, E., Weinke, G., Berger, A., and Puxbaum, H.: Arabitol and mannitol as tracers for the quantification of airborne fungal spores, Atmospheric Environment, 42, 588–593, https://doi.org/10.1016/j.atmosenv.2007.10.013, 2008.

https://doi.org/10.5194/egusphere-2026-1467
Preprint. Discussion started: 9 April 2026

Bazzano, A., Rivaro, P., Soggia, F., Ardini, F., and Grotti, M.: Anthropogenic and natural sources of particulate trace elements in the coastal marine environment of Kongsfjorden, Svalbard, Marine Chemistry, 163, 28–35, https://doi.org/10.1016/j.marchem.2014.04.001, 2014.

Bazzano, A., Ardini, F., Becagli, S., Traversi, R., Udisti, R., Cappelletti, D., and Grotti, M.: Source assessment of atmospheric lead measured at Ny-Ålesund, Svalbard, Atmospheric Environment, 113, 20–26, https://doi.org/10.1016/j.atmosenv.2015.04.053, 2015.

Bazzano, A., Cappelletti, D., Udisti, R., and Grotti, M.: Long-range transport of atmospheric lead reaching Ny-Ålesund: Inter-annual and seasonal variations of potential source areas, Atmospheric Environment, 139, 11–19, https://doi.org/10.1016/j.atmosenv.2016.05.026, 2016.

Bazzano, A., Bertinetti, S., Ardini, F., Cappelletti, D., and Grotti, M.: Potential Source Areas for Atmospheric Lead Reaching Ny-Ålesund from 2010 to 2018, Atmosphere, 12, 388, https://doi.org/10.3390/atmos12030388, 2021.

Becagli, S., Ghedini, C., Peeters, S., Rottiers, A., Traversi, R., Udisti, R., Chiari, M., Jalba, A., Despiau, S., Dayan, U., and Temara, A.: MBAS (Methylene Blue Active Substances) and LAS (Linear Alkylbenzene Sulphonates) in Mediterranean coastal aerosols: Sources and transport processes, Atmospheric Environment, 45, 6788–6801, https://doi.org/10.1016/j.atmosenv.2011.04.041, 2011.

Becagli, S., Amore, A., Caiazzo, L., Di Iorio, T. D., di Sarra, A., Lazzara, L., Marchese, C., Meloni, D., Mori, G., Muscari, G., Nuccio, C., Pace, G., Severi, M., and Traversi, R.: Biogenic aerosol in the Arctic from eight years of MSA data from Ny Ålesund (Svalbard Islands) and Thule (Greenland), Atmosphere, 10, 1–12, https://doi.org/10.3390/atmos10070349, 2019.

Becagli, S., Caiazzo, L., Di Iorio, T., di Sarra, A., Meloni, D., Muscari, G., Pace, G., Severi, M., and Traversi, R.: New insights on metals in the Arctic aerosol in a climate changing world, Science of The Total Environment, 741, 140511, https://doi.org/10.1016/j.scitotenv.2020.140511, 2020.

Becherini, F., Vitale, V., Lupi, A., Stone, R. S., Salvatori, R., Salzano, R., di Carlo, P., Viola, A. P., and Mazzola, M.: Surface albedo and spring snow melt variations at Ny-Ålesund, Svalbard, Bull. of Atmos. Sci.& Technol., 2, 14, https://doi.org/10.1007/s42865-021-00043-8, 2021.

Bory, A. J.-M., Abouchami, W., Galer, S. J. G., Svensson, A., Christensen, J. N., and Biscaye, P. E.: A Chinese Imprint in Insoluble Pollutants Recently Deposited in Central Greenland As Indicated by Lead Isotopes, Environ. Sci. Technol., 48, 1451–1457, https://doi.org/10.1021/es4035655, 2014.

Caiazzo, L., Calzolai, G., Becagli, S., Severi, M., Amore, A., and Chiari, M.: Carbonaceous aerosol in Polar areas : First results and improve- ments of the sampling strategies, 1–20, 2021.

Campbell, J. L., Cureatz, D. J. T., Flannigan, E. L., Heirwegh, C. M., Maxwell, J. A., Russell, J. L., and Taylor, S. M.: The Guelph PIXE Software Package V, Nuclear Instruments and Methods in Physics Research Section B: Beam Interactions with Materials and Atoms, 499, 77–88, https://doi.org/10.1016/j.nimb.2021.05.004, 2021.

Cavalli, F., Viana, M., Yttri, K. E., Genberg, J., and Putaud, J.-P.: Toward a standardised thermal-optical protocol for measuring atmospheric organic and elemental carbon: the EUSAAR protocol, Atmospheric Measurement Techniques, 3, 79–89, https://doi.org/10.5194/amt-3-79-2010, 2010.

Chiari, M., Barone, S., Bombini, A., Calzolai, G., Carraresi, L., Castelli, L., Czelusniak, C., Fedi, M. E., Gelli, N., Giambi, F., Giardi, F., Giuntini, L., Lagomarsino, S., Liccioli, L., Lucarelli, F., Manetti, M., Massi, M., Mazzinghi, A., Nava, S., Ottanelli, P., Sciortino, S., Ruberto, C., Sodi, L., Taccetti, F., and Mandò, P. A.: LABEC, the INFN ion beam laboratory of nuclear

https://doi.org/10.5194/egusphere-2026-1467
Preprint. Discussion started: 9 April 2026

techniques for environment and cultural heritage, Eur. Phys. J. Plus, 136, 472, https://doi.org/10.1140/epjp/s13360-021-01411-1, 2021.

Conca, E., Abollino, O., Giacomino, A., Buoso, S., Traversi, R., Becagli, S., Grotti, M., and Malandrino, M.: Source identification and temporal evolution of trace elements in PM10 collected near to Ny-Ålesund (Norwegian Arctic), Atmospheric Environment, 203, 153–165, https://doi.org/10.1016/j.atmosenv.2019.02.001, 2019.

Esau, I. and Sorokina, S.: Climatology of the arctic planetary boundary layer, Atmospheric Turbulence, Meteorological Modeling and Aerodynamics, edited by: Lang, PR and Lombargo, FS, Nova Science Publishers, Inc., New York, 3–58, 2009.

Fabbri, D., Torri, C., Simoneit, B. R. T., Marynowski, L., Rushdi, A. I., and Fabiańska, M. J.: Levoglucosan and other cellulose and lignin markers in emissions from burning of Miocene lignites, Atmospheric Environment, 43, 2286–2295, https://doi.org/10.1016/j.atmosenv.2009.01.030, 2009.

Feltracco, M., Barbaro, E., Tedeschi, S., Spolaor, A., Turetta, C., Vecchiato, M., Morabito, E., Zangrando, R., Barbante, C., and Gambaro, A.: Interannual variability of sugars in Arctic aerosol: Biomass burning and biogenic inputs, Science of the Total Environment, 706, https://doi.org/10.1016/j.scitotenv.2019.136089, 2020.

Feltracco, M., Barbaro, E., Spolaor, A., Vecchiato, M., Callegaro, A., Burgay, F., Vardè, M., Maffezzoli, N., Dallo, F., Scoto, F., Zangrando, R., Barbante, C., and Gambaro, A.: Year-round measurements of size-segregated low molecular weight organic acids in Arctic aerosol, Science of The Total Environment, 763, 142954, https://doi.org/10.1016/j.scitotenv.2020.142954, 2021.

Giannoni, M., Calzolai, G., Chiari, M., Cincinelli, A., Lucarelli, F., Martellini, T., and Nava, S.: A comparison between thermal-optical transmittance elemental carbon measured by different protocols in PM2.5 samples, Science of The Total Environment, 571, 195–205, https://doi.org/10.1016/j.scitotenv.2016.07.128, 2016.

Giardi, F., Becagli, S., Traversi, R., Frosini, D., Severi, M., Caiazzo, L., Ancillotti, C., Cappelletti, D., Moroni, B., Grotti, M., Bazzano, A., Lupi, A., Mazzola, M., Vitale, V., Abollino, O., Ferrero, L., Bolzacchini, E., Viola, A., and Udisti, R.: Size distribution and ion composition of aerosol collected at Ny-Ålesund in the spring–summer field campaign 2013, Rendiconti Lincei, 27, 47–58, https://doi.org/10.1007/s12210-016-0529-3, 2016.

Gilardoni, S., Lupi, A., Mazzola, M., Michele, C. D., Moroni, B., Ferrero, L., Markuszewski, P., Rozwadowska, A., Krejci, R., Zieger, P., Tunved, P., Karlsson, L., Vratolis, S., Eleftheriadis, K., and Viola, A.: Atmospheric black carbon in Svalbard, Svalbard Integrated Arctic Earth Observing System, https://doi.org/10.5281/zenodo.4707201, 2020.

Gilardoni, S., Heslin-Rees, D., Mazzola, M., Vitale, V., Sprenger, M., and Krejci, R.: Drivers controlling black carbon temporal variability in the lower troposphere of the European Arctic, Atmos. Chem. Phys., 23, 15589–15607, https://doi.org/10.5194/acp-23-15589-2023, 2023.

Grotti, M., Vecchio, M. A., Gobbato, D., Mataloni, M., and Ardini, F.: Precise determination of ^{204}Pb-based isotopic ratios in environmental samples by quadrupole inductively coupled plasma mass spectrometry, J. Anal. At. Spectrom., 38, 1057–1064, https://doi.org/10.1039/D2JA00424K, 2023.

Grotti, M., Ardini, F., Vecchio, M. A., Mataloni, M., Bertinetti, S., Bruschi, F., Moroni, B., Cappelletti, D., Hobin, K., and Vanhaecke, F.: New insights into the sources of atmospheric lead reaching the Arctic by isotopic analysis of PM10 atmospheric particles and resuspended soils, Atmospheric Environment, 330, 120541, https://doi.org/10.1016/j.atmosenv.2024.120541, 2024.

https://doi.org/10.5194/egusphere-2026-1467
Preprint. Discussion started: 9 April 2026

Groot Zwaaftink CD, Grythe H., Skov H., Sthol A.: Substantial contribution of northern high-latitude sources to mineral dust in the Arctic, JGR Atmospheres, 121, 13,678-13,697, https://doi.org/10.1002/2016JD025482, 2016.
Hans Wedepohl, K.: The composition of the continental crust, Geochimica et Cosmochimica Acta, 59, 1217–1232, https://doi.org/10.1016/0016-7037(95)00038-2, 1995.

Henderson, P. and Henderson, G. M.: Earth science data, Cambridge University Press, 92–97 pp., 2009.

Huang, J. and Jaeglé, L.: Wintertime enhancements of sea salt aerosol in polar regions consistent with a sea ice source from blowing snow, Atmospheric Chemistry and Physics, 17, 3699–3712, https://doi.org/10.5194/acp-17-3699-2017, 2017.

IPCC: Summary for Policymakers, in: Climate Change 2013: The Physical Science Basis. Contribution of Working Group I to the Fifth Assessment Report of the Intergovernmental Panel on Climate Change, edited by: Stocker, T. F., Qin, D., Plattner, G.-K., Tignor, M., Allen, S. K., Boschung, J., Nauels, A., Xia, Y., Bex, V., and Midgley, P. M., Cambridge, United Kingdom and New York, NY, USA, 2013.

Jozef, G. C., Cassano, J. J., Dahlke, S., Dice, M., Cox, C. J., and de Boer, G.: An overview of the vertical structure of the atmospheric boundary layer in the central Arctic during MOSAiC, Atmospheric Chemistry and Physics, 24, 1429–1450, https://doi.org/10.5194/acp-24-1429-2024, 2024.

Kyllönen, K., Vestenius, M., Anttila, P., Makkonen, U., Aurela, M., Wängberg, I., Nerentorp Mastromonaco, M., and Hakola, H.: Trends and source apportionment of atmospheric heavy metals at a subarctic site during 1996–2018, Atmospheric Environment, 236, 117644, https://doi.org/10.1016/J.ATMOSENV.2020.117644, 2020.

Lunder Halvorsen, H., Aspmo Pfaffhuber, K., Nipen, M., Bohlin-Nizzetto, P., Flatlandsmo Berglen, T., Nikiforov, V., and Hartz, W. F.: Monitoring of environmental contaminants in air and precipitation. Annual report 2024, NILU, 2025.

Mazzola, M., Busetto, M., Ferrero, L., Viola, A. P., and Cappelletti, D.: AGAP: an atmospheric gondola for aerosol profiling, Rendiconti Lincei, 27, 105–113, https://doi.org/10.1007/s12210-016-0514-x, 2016.

Mukai, H., Machida, T., Tanaka, A., Vera, Y. P., and Uematsu, M.: Lead isotope ratios in the urban air of eastern and central Russia, Atmospheric Environment, 35, 2783–2793, https://doi.org/10.1016/S1352-2310(00)00341-1, 2001.

Müller, T., Henzing, J. S., De Leeuw, G., Wiedensohler, A., Alastuey, A., Angelov, H., Bizjak, M., Collaud Coen, M., Engström, J. E., Gruening, C., Hillamo, R., Hoffer, A., Imre, K., Ivanow, P., Jennings, G., Sun, J. Y., Kalivitis, N., Karlsson, H., Komppula, M., Laj, P., Li, S.-M., Lunder, C., Marinoni, A., Martins Dos Santos, S., Moerman, M., Nowak, A., Ogren, J. A., Petzold, A., Pichon, J. M., Rodriquez, S., Sharma, S., Sheridan, P. J., Teinilä, K., Tuch, T., Viana, M., Virkkula, A., Weingartner, E., Wilhelm, R., and Wang, Y. Q.: Characterization and intercomparison of aerosol absorption photometers: result of two intercomparison workshops, Atmos. Meas. Tech., 4, 245–268, https://doi.org/10.5194/amt-4-245-2011, 2011.

Nayebare, S. R., Aburizaiza, O. S., Siddique, A., Carpenter, D. O., Hussain, M. M., Zeb, J., Aburiziza, A. J., and Khwaja, H. A.: Ambient air quality in the holy city of Makkah: A source apportionment with elemental enrichment factors (EFs) and factor analysis (PMF), Environmental Pollution, 243, 1791–1801, https://doi.org/10.1016/j.envpol.2018.09.086, 2018.

Park, K.-T., Yoon, Y. J., Lee, K., Tunved,P., Krejci, R., Ström, J., Jang, E., Kang, H.J., Jang, S., Park, J., Lee, B. Y., Traversi, R., Becagli, S., Hermansen, O. : Dimethyl sulfide-induced increase in cloud condensation nuclei in the Arctic atmosphere, Global Biogeochemical Cycles, 35, e2021GB006969. https://doi.org/10.1029/2021GB006969, 2021.

Platt, S. M., Hov, Ø., Berg, T., Breivik, K., Eckhardt, S., Eleftheriadis, K., Evangeliou, N., Fiebig, M., Fisher, R., Hansen, G., Hansson, H. C., Heintzenberg, J., Hermansen, O., Heslin-Rees, D., Holmén, K., Hudson, S., Kallenborn, R., Krejci, R., Krognes, T., Larssen, S., Lowry, D., Myhre, C. L., Lunder, C., Nisbet, E., Nizzetto, P. B., Park, K. T., Pedersen, C. A.,

https://doi.org/10.5194/egusphere-2026-1467
Preprint. Discussion started: 9 April 2026

Pfaffhuber, K. A., Röckmann, T., Schmidbauer, N., Solberg, S., Stohl, A., Ström, J., Svendby, T., Tunved, P., Tørnkvist, K., Van Der Veen, C., Vratolis, S., Yoon, Y. J., Yttri, K. E., Zieger, P., Aas, W., and Tørseth, K.: Atmospheric composition in the European Arctic and 30 years of the Zeppelin Observatory, Ny-Ålesund, Atmospheric Chemistry and Physics, 22, 3321–3369, https://doi.org/10.5194/ACP-22-3321-2022, 2022.

Rader, F., Traversi, R., Severi, M., Becagli, S., Müller, K.-J., Nakoudi, K., and Ritter, C.: Overview of Aerosol Properties in the European Arctic in Spring 2019 Based on In Situ Measurements and Lidar Data, Atmosphere, 12, 271, https://doi.org/10.3390/atmos12020271, 2021.

Rhodes, R. H., Yang, X., and Wolff, E. W.: Sea Ice Versus Storms: What Controls Sea Salt in Arctic Ice Cores?, Geophysical Research Letters, 45, 5572–5580, https://doi.org/10.1029/2018GL077403, 2018.

Schmidl, C., Marr, I. L., Caseiro, A., Kotianová, P., Berner, A., Bauer, H., Kasper-Giebl, A., and Puxbaum, H.: Chemical characterisation of fine particle emissions from wood stove combustion of common woods growing in mid-European Alpine regions, Atmospheric Environment, 42, 126–141, https://doi.org/10.1016/j.atmosenv.2007.09.028, 2008.

Serreze, M. C. and Barry, R. G.: Processes and impacts of Arctic amplification: A research synthesis, Global and Planetary Change, 77, 85–96, https://doi.org/10.1016/j.gloplacha.2011.03.004, 2011.

Shotyk, W., Zheng, J., Krachler, M., Zdanowicz, C., Koerner, R., and Fisher, D.: Predominance of industrial Pb in recent snow (1994–2004) and ice (1842–1996) from Devon Island, Arctic Canada, Geophysical Research Letters, 32, https://doi.org/10.1029/2005GL023860, 2005.

Simoneit, B. R. T.: A review of biomarker compounds as source indicators and tracers for air pollution, Environmental Science and Pollution Research, 6, 159–169, https://doi.org/10.1007/bf02987621, 1999.

Spagnesi, A., Barbaro, E., Feltracco, M., Scoto, F., Vecchiato, M., Vardè, M., Mazzola, M., Burgay, F., Bruschi, F., Hoppe, C. J. M., Bailey, A., Gambaro, A., Barbante, C., and Spolaor, A.: Seasonal and interannual variability on the chemical composition of the Svalbard surface snowpack, Atmos. Chem. Phys., 25, 16215–16232, https://doi.org/10.5194/acp-25-16215-2025, 2025.

Stein, A. F., Draxler, R. R., Rolph, G. D., Stunder, B. J. B., Cohen, M. D., and Ngan, F.: Noaa's hysplit atmospheric transport and dispersion modeling system, Bulletin of the American Meteorological Society, 96, 2059–2077, https://doi.org/10.1175/BAMS-D-14-00110.1, 2015.

Stohl, A.: Characteristics of atmospheric transport into the Arctic troposphere, J. Geophys. Res., 111, 2005JD006888, https://doi.org/10.1029/2005JD006888, 2006a.

Stohl, A.: Characteristics of atmospheric transport into the Arctic troposphere, Journal of Geophysical Research: Atmospheres, 111, D11306, https://doi.org/10.1029/2005JD006888, 2006b.

Ström, J., Engvall, A. C., Delbart, F., Krejci, R., and Treffeisen, R.: On small particles in the Arctic summer boundary layer: observations at two different heights near Ny-Ålesund, Svalbard, Tellus B: Chemical and Physical Meteorology, 61, 473–482, https://doi.org/10.1111/j.1600-0889.2009.00412.x, 2009.

Sturges, William Thomas, and L. A. Barrie. "Stable lead isotope ratios in arctic aerosols: evidence for the origin of arctic air pollution." Atmospheric Environment, 23.11 (1989): 2513-2519, https://doi.org/10.1016/0004-6981(89)90263-1, 1967.

Sturges, W. T., Hopper, J. F., Barrie, L. A., and Schnell, R. C.: Stable lead isotope ratios in Alaskan arctic aerosols, Atmospheric Environment. Part A. General Topics, 27, 2865–2871, https://doi.org/10.1016/0960-1686(93)90317-R, 1993.

https://doi.org/10.5194/egusphere-2026-1467
Preprint. Discussion started: 9 April 2026

Traversi, R., Becagli, S., Severi, M., Caiazzo, L., Mazzola, M., Lupi, A., Fiebig, M., Hermansen, O., Krejci, R., and Unit, A. S.: Arctic haze in a climate changing world: the 2010- 2020 trend (HAZECLIC) 4, Svalbard Integrated Arctic Earth Observing System, Longyearbyen, 2021.

Tunved, P., Ström, J., and Krejci, R.: Arctic aerosol life cycle: linking aerosol size distributions observed between 2000 and 2010 with air mass transport and precipitation at Zeppelin station, Ny-Ålesund, Svalbard, Atmospheric Chemistry and Physics, 13, 3643–3660, https://doi.org/10.5194/acp-13-3643-2013, 2013.

Udisti, R., Bazzano, A., Becagli, S., Bolzacchini, E., Caiazzo, L., Cappelletti, D., Ferrero, L., Frosini, D., Giardi, F., Grotti, M., Lupi, A., Malandrino, M., Mazzola, M., Moroni, B., Severi, M., Traversi, R., Viola, A., and Vitale, V.: Sulfate source apportionment in the Ny-Ålesund (Svalbard Islands) Arctic aerosol, Rendiconti Lincei, 27, 85–94, https://doi.org/10.1007/s12210-016-0517-7, 2016.

Udisti, R., Traversi, R., and Becagli, S.: Arctic Aerosols in: Physics and Chemistry of the Arctic Atmosphere, edited by: Kokhanovsky, AA and Tomasi, C, 2020.

Wentworth, G. R., Murphy, J. G., Croft, B., Martin, R. V., Pierce, J. R., Côté, J.-S., Courchesne, I., Tremblay, J.-É., Gagnon, J., Thomas, J. L., Sharma, S., Toom-Sauntry, D., Chivulescu, A., Levasseur, M., and Abbatt, J. P. D.: Ammonia in the summertime Arctic marine boundary layer: sources, sinks, and implications, Atmos. Chem. Phys., 16, 1937–1953, https://doi.org/10.5194/acp-16-1937-2016, 2016.

Wong, M. Y., Rathod, S. D., Marino, R., Li, L., Howarth, R. W., Alastuey, A., Alaimo, M. G., Barraza, F., Carneiro, M. C., Chellam, S., Chen, Y. C., Cohen, D. D., Connelly, D., Dongarra, G., Gómez, D., Hand, J., Harrison, R. M., Hopke, P. K., Hueglin, C., Kuang, Y. wen, Lambert, F., Liang, J., Losno, R., Maenhaut, W., Milando, C., Monteiro, M. I. C., Morera-Gómez, Y., Querol, X., Rodríguez, S., Smichowski, P., Varrica, D., Xiao, Y. hua, Xu, Y., and Mahowald, N. M.: Anthropogenic Perturbations to the Atmospheric Molybdenum Cycle, Global Biogeochemical Cycles, 35, e2020GB006787, https://doi.org/10.1029/2020GB006787, 2021.

Yttri, K. E., Bäcklund, A., Conen, F., Eckhardt, S., Evangeliou, N., Fiebig, M., Kasper-Giebl, A., Gold, A., Gundersen, H., Myhre, C. L., Platt, S. M., Simpson, D., Surratt, J. D., Szidat, S., Rauber, M., Tørseth, K., Ytre-Eide, M. A., Zhang, Z., and Aas, W.: Composition and sources of carbonaceous aerosol in the European Arctic at Zeppelin Observatory, Svalbard (2017 to 2020), Atmospheric Chemistry and Physics, 24, 2731–2758, https://doi.org/10.5194/acp-24-2731-2024, 2024.

Yus-Díez, J., Bernardoni, V., Močnik, G., Alastuey, A., Ciniglia, D., Ivančič, M., Querol, X., Perez, N., Reche, C., Rigler, M., Vecchi, R., Valentini, S., and Pandolfi, M.: Determination of the multiple-scattering correction factor and its cross-sensitivity to scattering and wavelength dependence for different AE33 Aethalometer filter tapes: a multi-instrumental approach, Atmos. Meas. Tech., 14, 6335–6355, https://doi.org/10.5194/amt-14-6335-2021, 2021.

Zhan, J., Li, W., Chen, L., Lin, Q., and Gao, Y.: Anthropogenic influences on aerosols at Ny-Ålesund in the summer Arctic, Atmospheric Pollution Research, 8, 383–393, https://doi.org/10.1016/j.apr.2016.10.010, 2017.